Dear Author,

Here are the proofs of your article.

- You can submit your corrections **online**, via **e-mail** or by **fax**.
- For **online** submission please insert your corrections in the online correction form. Always indicate the line number to which the correction refers.
- You can also insert your corrections in the proof PDF and **email** the annotated PDF.
- For fax submission, please ensure that your corrections are clearly legible. Use a fine black pen and write the correction in the margin, not too close to the edge of the page.
- Remember to note the **journal title**, **article number**, and **your name** when sending your response via e-mail or fax.
- **Check** the metadata sheet to make sure that the header information, especially author names and the corresponding affiliations are correctly shown.
- **Check** the questions that may have arisen during copy editing and insert your answers/ corrections.
- **Check** that the text is complete and that all figures, tables and their legends are included. Also check the accuracy of special characters, equations, and electronic supplementary material if applicable. If necessary refer to the *Edited manuscript*.
- The publication of inaccurate data such as dosages and units can have serious consequences. Please take particular care that all such details are correct.
- Please **do not** make changes that involve only matters of style. We have generally introduced forms that follow the journal's style.
  Substantial changes in content, e.g., new results, corrected values, title and authorship are not allowed without the approval of the responsible editor. In such a case, please contact the Editorial Office and return his/her consent together with the proof.
- If we do not receive your corrections **within 48 hours**, we will send you a reminder.
- Your article will be published **Online First** approximately one week after receipt of your corrected proofs. This is the **official first publication** citable with the DOI. **Further changes are, therefore, not possible.**
- The **printed version** will follow in a forthcoming issue.

Please note

After online publication, subscribers (personal/institutional) to this journal will have access to the complete article via the DOI using the URL: http://dx.doi.org/[DOI].
If you would like to know when your article has been published online, take advantage of our free alert service. For registration and further information go to: http://www.springerlink.com.

Due to the electronic nature of the procedure, the manuscript and the original figures will only be returned to you on special request. When you return your corrections, please inform us if you would like to have these documents returned.

Metadata of the article that will be visualized in OnlineFirst

ArticleTitle	~~Pan-European~~ ground-motion prediction equations for the average horizontal component of PGA, PGV, and 5 %-damped PSA at spectral periods up to 3.0 s using the RESORCE dataset	
Article Sub-Title		
Article CopyRight	Springer Science+Business Media Dordrecht (This will be the copyright line in the final PDF)	
Journal Name	Bulletin of Earthquake Engineering	
Corresponding Author	Family Name	**Bindi**
	Particle	
	Given Name	**D.**
	Suffix	
	Division	Helmholtz Centre Potsdam GFZ
	Organization	German Research Centre for Geosciences
	Address	Helmholtzstraße 7, Potsdam, 14467 , Germany
	Email	~~bindi@mi.ingv.it~~
Author	Family Name	**Massa**
	Particle	
	Given Name	**M.**
	Suffix	
	Division	
	Organization	Istituto Nazionale di Geofisica e Vulcanologia
	Address	via Bassini 15, Milano, 20133 , Italy
	Email	
Author	Family Name	**Luzi**
	Particle	
	Given Name	**L.**
	Suffix	
	Division	
	Organization	Istituto Nazionale di Geofisica e Vulcanologia
	Address	via Bassini 15, Milano, 20133 , Italy
	Email	
Author	Family Name	**Ameri**
	Particle	
	Given Name	**G.**
	Suffix	
	Division	
	Organization	FUGRO-Geoter
	Address	Auriol, 13390 , France
	Email	
Author	Family Name	**Pacor**
	Particle	
	Given Name	**F.**
	Suffix	

	Division	
	Organization	Istituto Nazionale di Geofisica e Vulcanologia
	Address	via Bassini 15, Milano, 20133 , Italy
	Email	
Author	Family Name	**Puglia**
	Particle	
	Given Name	**R.**
	Suffix	
	Division	
	Organization	Istituto Nazionale di Geofisica e Vulcanologia
	Address	via Bassini 15, Milano, 20133 , Italy
	Email	
Author	Family Name	**Augliera**
	Particle	
	Given Name	**P.**
	Suffix	
	Division	
	Organization	Istituto Nazionale di Geofisica e Vulcanologia
	Address	via Bassini 15, Milano, 20133 , Italy
	Email	

	Received	22 December 2012
Schedule	Revised	
	Accepted	16 September 2013

Abstract

This article presents a set of ~~Pan-European~~ Ground-Motion Prediction Equations (GMPEs) derived from the RESORCE strong motion data bank, following a standard regression approach. The parametric GMPEs are derived for the peak ground acceleration, peak ground velocity, and 5 %-damped pseudo-absolute acceleration response spectra computed over 23 periods between 0.02 and 3 s, considering the average horizontal-component ground-motions. The GMPEs are valid for distances less than 300 km, hypocentral depth up to 35 km and over the magnitude range 4–7.6. Two metrics for the source-to-station distance (i.e. Joyner-Boore and hypocentral) are considered. The selected dataset is composed by 2,126 recordings (at a period of 0.1 s) related to 365 earthquakes,that includes strong-motion data from 697 stations.The EC8 soil classification (four classes from A to D) discriminates recording sites and four classes (normal, reverse, strike-slip, and unspecified) describe the style of faulting. A subset which contains only stations with measured Vs30 and earthquakes with specified focal mechanism (1,224 records from 345 stations and 255 earthquakes) is used to test of the accuracy of the median prediction and the variability associated to the broader data set. A random effect regression scheme is applied and bootstrap analyses are performed to estimate the 95 % confidence levels for the parameters. The total standard deviation sigma is decomposed into between-events and within-event components, and the site-to-site component is evaluated as well. The results show that the largest contribution to the total sigma is coming from the within-event component. When analyzing the residual distributions, no significant trends are observed that can be ascribed to the earthquake type (mainshock-aftershock classification) or to the non-linear site amplifications. The proposed GMPEs have lower median values than global models at short periods and large distances, while are consistent with global models at long periods $(T > 1)$ s. Consistency is found with two regional models developed for Turkey and Italy, as the considered dataset is dominated by waveforms recorded in these regions.

Keywords (separated by '-') Ground motion prediction equation - Europe - RESORCE data set

Footnote Information **Electronic supplementary material** The online version of this article (doi:10.1007/s10518-013-9525-5) contains supplementary material, which is available to authorized users.

Metadata of the article that will be visualized in OnlineAlone

Electronic supplementary material	Below is the link to the electronic supplementary material. **MOESM1:** Supplementary material 1 (r 1332 KB). **MOESM2:** Supplementary material 2 (doc 22 KB). **MOESM3:** Supplementary material 3 (xls 85 KB). **MOESM4:** Supplementary material 4 (r 1381 KB).

Journal: 10518
Article: 9525

Author Query Form

Please ensure you fill out your response to the queries raised below and return this form along with your corrections

Dear Author

During the process of typesetting your article, the following queries have arisen. Please check your typeset proof carefully against the queries listed below and mark the necessary changes either directly on the proof/online grid or in the 'Author's response' area provided below

Query	Details required	Author's response
1.	References Umbria-Marche (1997), L'Aquila (2009) are cited in text but not provided in the reference list. Please provide references in the list or delete these citations.	1997-1998 Umbria-Marche and 2009 L'Aquila seismic sequences
2.	Please provide volume and page range for reference Akkar et al. (2013).	doi 10.1007/s10518-013-9461-4
3.	We have changed the Tables 1a, 1b, 2a, 2b, 3, 4a, 4b, 5a, 5b to Tables 1, 2, 3, 4, 5, 6, 7, 8, 9. Please check and confirm.	ok

Bull Earthquake Eng
DOI 10.1007/s10518-013-9525-5

ORIGINAL RESEARCH PAPER

~~Pan-European~~ ground-motion prediction equations for the average horizontal component of PGA, PGV, and 5 %-damped PSA at spectral periods up to 3.0 s using the RESORCE dataset

D. Bindi · M. Massa · L. Luzi · G. Ameri · F. Pacor · R. Puglia · P. Augliera

Received: 22 December 2012 / Accepted: 16 September 2013

Abstract This article presents a set of ~~Pan-European~~ Ground-Motion Prediction Equations (GMPEs) derived from the RESORCE strong motion data bank, following a standard regression approach. The parametric GMPEs are derived for the peak ground acceleration, peak ground velocity, and 5 %-damped pseudo-absolute acceleration response spectra computed over 23 periods between 0.02 and 3 s, considering the average horizontal-component ground-motions. The GMPEs are valid for distances less than 300 km, hypocentral depth up to 35 km and over the magnitude range 4–7.6. Two metrics for the source-to-station distance (i.e. Joyner-Boore and hypocentral) are considered. The selected dataset is composed by 2,126 recordings (at a period of 0.1 s) related to 365 earthquakes that includes strong-motion data from 697 stations.The EC8 soil classification (four classes from A to D) discriminates recording sites and four classes (normal, reverse, strike-slip, and unspecified) describe the style of faulting. A subset which contains only stations with measured Vs30 and earthquakes with specified focal mechanism (1,224 records from 345 stations and 255 earthquakes) is used to test of the accuracy of the median prediction and the variability associated to the broader data set. A random effect regression scheme is applied and bootstrap analyses are performed to estimate the 95 % confidence levels for the parameters. The total standard deviation sigma is decomposed into between-events and within-event components, and the site-to-site component is evaluated as well. The results show that the largest contribution to the total sigma is coming from the within-event component. When analyzing the residual distributions, no

---

Electronic supplementary material The online version of this article (doi:10.1007/s10518-013-9525-5) contains supplementary material, which is available to authorized users.

D. Bindi (✉)
Helmholtz Centre Potsdam GFZ, German Research Centre for Geosciences,
Helmholtzstraße 7, 14467 Potsdam, Germany
e-mail: ~~bindi@mi.ingv.it~~

M. Massa · L. Luzi · F. Pacor · R. Puglia · P. Augliera
Istituto Nazionale di Geofisica e Vulcanologia, via Bassini 15, 20133 Milano, Italy

G. Ameri
FUGRO-Geoter, 13390 Auriol, France

significant trends are observed that can be ascribed to the earthquake type (mainshock-aftershock classification) or to the non-linear site ~~amplifications~~. The proposed GMPEs have lower median values than global models at short periods and large distances, while are consistent with global models at long periods (T > 1) s. Consistency is found with two regional models developed for Turkey and Italy, as the considered dataset is dominated by waveforms recorded in these regions.

Keywords Ground motion prediction equation · Europe · RESORCE data set

1 Introduction

In the framework of the FP7 EU project SHARE (http://www.share-eu.org/), Yener et al. (2010) compiled a new databank for hazard studies in Europe. The SHARE databank is a collection of records and metadata contained in previously compiled databases with a ranking of preferred metadata in case of data overlaps and no waveform processing. The SHARE databank was then exploited by the SIGMA project (http://projet-sigma.com/organisation.html), in order to improve the seismic hazard assessment in France. A new databank (hereafter referred to as RESORCE) has been compiled, from the subset of European data included in SHARE after metadata revision and uniform re-processing of waveforms (Akkar et al. 2013).

The RESORCE databank has been used by different authors to derive a set of ground-motion models following different approaches (Douglas et al. 2013). In this article, we first describe the data selection applied to RESORCE for deriving ~~Pan-European~~ GMPEs and we introduce the functional form, along with the explanatory variables considered in the regressions. The results, provided in terms of coefficients of the equations and associated 95 % confidence levels, are discussed through a comparison with previously derived global and regional models and analyzing the residual distributions. A comprehensive comparison among the different models derived from RESORCE is presented in Douglas et al. (2013).

2 Flat file compilation from the RESORCE data bank

The RESORCE databank (Akkar et al. 2013) originally includes 5,882 waveforms from 1814 earthquakes occurred in Europe and Middle East from 1967 to 2011 in the magnitude range from 2.8 to 7.8 (the largest magnitude is relevant to the 1969/02/28 02:40:31 Portugal, offshore single-recorded earthquake). In this study no additional analyses are performed to identify poor quality data and a preliminary selection is made in order to exclude: (i) unprocessed records, (ii) data lacking the three components of ground-motion and (iii) earthquakes for which moment magnitude is not provided. Events with unreliable magnitude are also disregarded.

The following criteria are adopted to select the records for the regression:

- *Range of validity.* Given the recent interest in considering small magnitude earthquakes for assessing the hazard in several regions of Europe (http://projet-sigma.com/ScientificObjectives.html), records from events with moment magnitudes larger than or equal to four are considered. Hypocentral depths are lower than 35 km and distances (Joyner-Boore, R_{jb}, or epicentral R_{epi}) shorter than 300 km. The epicentral distance, R_{epi}, is used to approximate R_{jb} when the latter is unspecified, but only when $M \leq 5$ and

$R_{epi} \geq 10$ km. For larger magnitudes and smaller epicentral distances, records without R_{jb} are disregarded.

- *Waveform selection*. Only records filtered with low-pass corner frequency larger than or equal to 20 Hz and, for each period T, only recordings filtered with high-pass corner frequency $f_{hp} \leq 1/(1.25\,T)$ are considered.
- *Sampling*. Single recorded earthquakes are not selected.

  Two different subsets of data are then compiled, based on the information available about site classification and style of faulting:
- *DS-EC8 dataset*. It is composed by waveforms recorded by stations characterized by EC8 site classes (CEN 2004), which are based on the average shear-wave velocity of the uppermost 30 m, Vs30 (class A: $Vs30 \geq 800$ m/s, class B: $360 \leq Vs30 \leq 800$ m/s, class C: $180 \leq Vs30 \leq 360$ m/s, class D: $Vs30 \leq 180$ m/s and class E: 5–20 m of C or D-type alluvium underlain by stiffer material with $Vs30 \geq 800$ m/s).

  The RESORCE site categories are determined either from shear wave velocity profiles or inferred by surface geology and, among them, only classes from A to D are accounted for, as only few stations (less than 5) are classified as class E. Waveforms from events with unspecified focal mechanism are included in DS-EC8. This data set contains 2,126 recordings from 365 earthquakes and 697 stations.
- *DS-VS30 dataset*. It is composed by waveforms recorded by stations with measured Vs30 and relative to events with known focal mechanism. It contains 1,224 recordings relevant to 255 earthquakes recorded by 345 stations.

Figure 1 shows the magnitude-distance distribution of the two datasets at $T = 0.1$ s. Each individual magnitude-distance entity is shown in the left panel, where different colors indicate different networks, whereas the right panel shows the hit counts, computed over a grid where the distance is discretized into 30 bins, equally spaced over a logarithmic scale from 1 to 300 km, and the magnitude range is discretized into 0.15 unit intervals. The bulk of the selected data sets is represented by Italian and Turkish data, that mainly cover the magnitude range from 4 to 6.5 and the distance range from 10 to 200 km. The data set includes sixteen events with magnitude larger than 6.5, seven of which having magnitude larger than 7.

Figure 2 shows the distribution of site categories and focal mechanisms for the two datasets. The main features of the DS-EC8 are shown in the upper left panel, which indicates that categories A, B and C characterize the Italian dataset, while Turkish data have been mainly recorded by stations belonging to soil category B and C. When data characterized by shear wave velocity profiles are selected (DS-VS30, lower left panel) there is a strong reduction of class A and a relative increase of Turkish data, as the majority of European networks lack of detailed site characterization.

The style of faulting distribution is shown in Fig. 2 (top right panel for DS-EC8 and bottom right panel for DS-VS30). Normal and strike-slip mechanisms, that are the bulk of the Italian and Turkish datasets, are the most represented. The relative proportion of waveforms from normal and strike-slip style of faulting does not change in the two datasets, although there is a considerable reduction of Italian normal events in DS-VS30.

Since we consider only the spectral ordinates within the usable frequency band, which is function of the low-cut frequency, the number of selected recordings varies with period and, in particular, decreases with increasing periods, as detailed in Fig. 3 for the DS-EC8 dataset. The number of selected recordings, stations and earthquakes for $T = 0.1$ s are 2,126, 697 and 365, respectively. At 3 s the recordings decrease relevantly being 1,460, from 580 stations and 226 earthquakes. Figure 3 (right) displays the plot of the low cut filter corner in function of the earthquake magnitude for the available data set, which indicates that some of the small

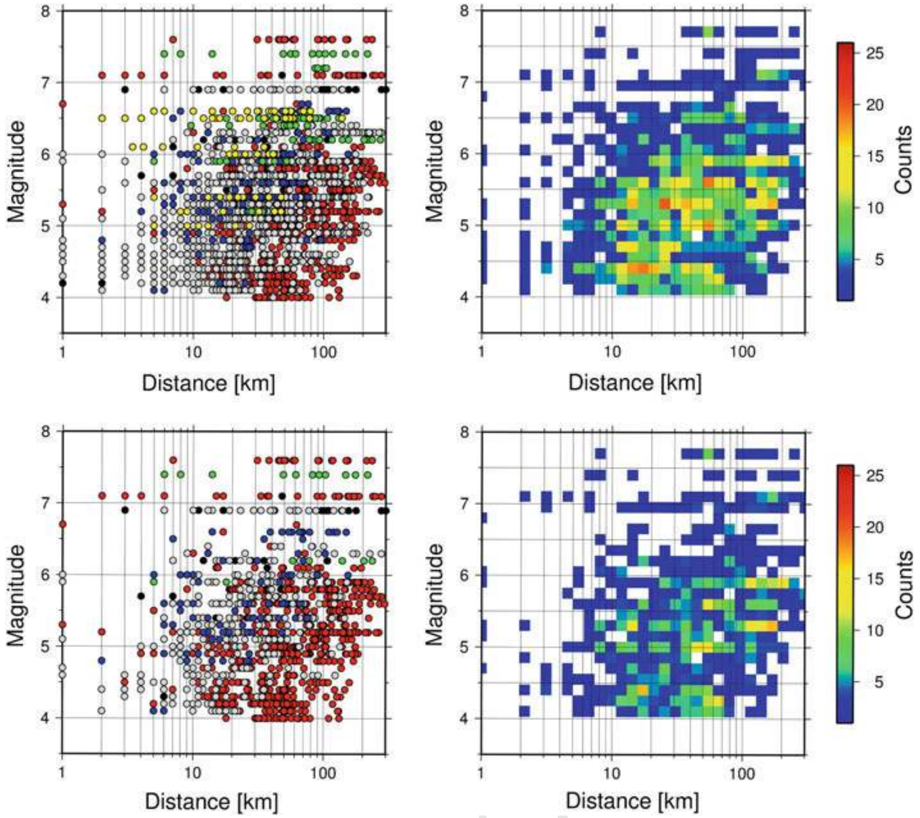

Fig. 1 ~~Right~~ *panels*: Magnitude versus distance scatter plot for DS-EC8 (*top*) and DS-V~~s~~30 (*bottom*) at T = 0.1 s. The records are colour coded accordingly to the network: *red* (Turkey); *gray* (Italy); *blue* (Greece); *green* (Iran); *yellow* (Iceland); *black* (other countries). ~~Left~~ *panels*: hit counts computed for the data distribution shown in the *left panels*, discretizing the distance range (1–300 km) into 30 equally spaced bins over a logarithmic scale and considering 0.15 magnitude unit intervals

magnitude events have low filter corners and, therefore, noise at long periods could still be present in the waveforms after processing.

3 Functional form and regression

The GMPEs are derived considering a parametric model based on the following functional form (e.g. Boore and Atkinson 2008; Akkar and Cagnan 2010; Bindi et al. 2011a)

$$\log_{10} Y = e_1 + F_D(R, M) + F_M(M) + F_S + F_{sof} \tag{1}$$

where the distance F_D and magnitude F_M functions are given by:

$$F_D(R, M) = \left[c_1 + c_2\left(M - M_{ref}\right)\right]\log_{10}\left(\sqrt{R^2 + h^2}/R_{ref}\right) - c_3\left(\sqrt{R^2 + h^2} - R_{ref}\right) \tag{2}$$

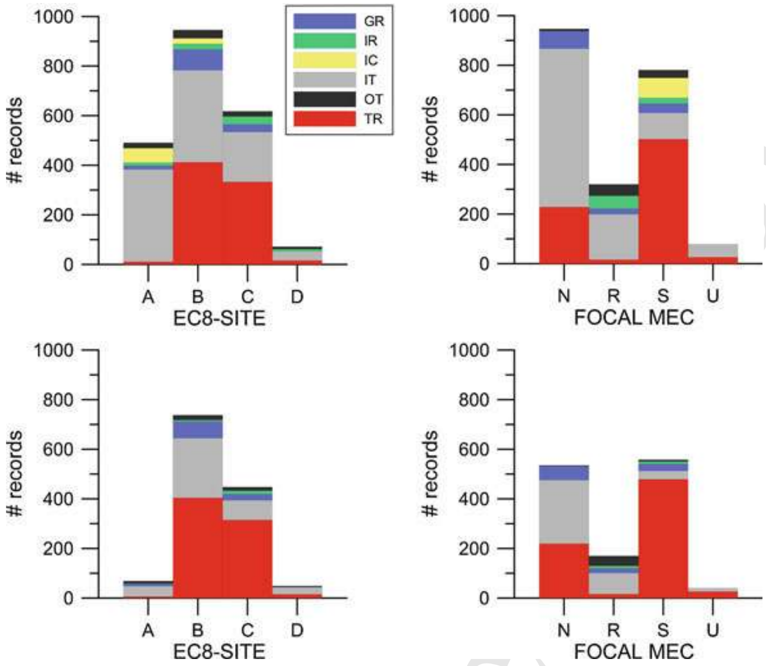

Fig. 2 EC8 site categories (*right*) and style-of-faulting (*left*) distributions for the DS-EC8 (*top*) and DS-Vs30 (*bottom*) datasets at T = 0.1 s. *Different colours* indicate different countries

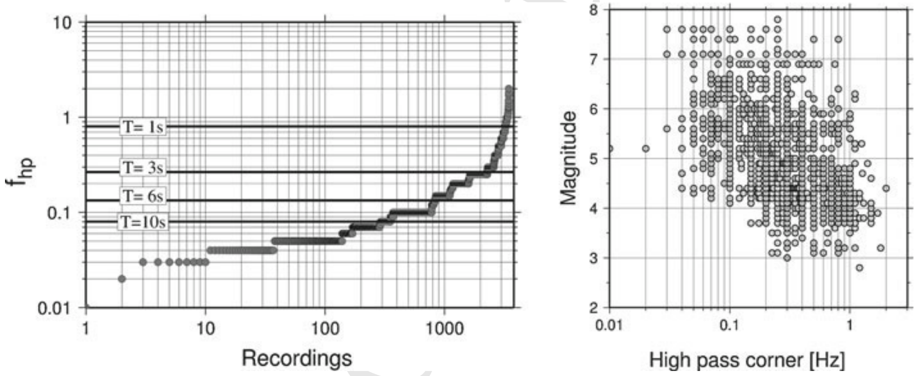

Fig. 3 *Left*: Number of recordings (abscissa) as function of the high-pass corner frequency (ordinate). The selections, considering f = 1/(1.25 T), at T = 1, 3, 6 and 10 s, are indicated. *Right*: Magnitude versus corner frequency scatter plot, considering the high-pass filter applied to the original data set

$$F_M(M) = \begin{cases} b_1\,(M - M_h) + b_2\,(M - M_h)^2 & \text{for } M \le M_h \\ b_3\,(M - M_h) & \text{otherwise} \end{cases} \tag{3}$$

Preliminary analysis about the data scaling with magnitude and distance confirmed the suitability of the selected functional form to describe the dependences of the ground-motion parameters on the explanatory variables. Following Bommer and Akkar (2012), the regressions are performed considering both a point-source and an extended-source measure of the source-to-site distance R, namely the Joyner and Boore distance R_{JB} and the hypocentral distance R_{hypo}. Additional explanatory variables related to the source model (e.g. hanging/foot walls effect; depth to the top of the rupture; etc.) or other measure for the source-to-station distance (e.g. distance from the rupture) are not considered because of the lack of information in RESORCE.

The functional form F_S in Eq. (1) represents the site amplification. The model derived in this article includes only a linear site amplification term although nonlinear site effects are expect to be important for strong shaking at soil sites, that is for large and close earthquakes recorded at site with low Vs30 values (e.g. classes C and D of EC8). Unfortunately these conditions are not well sampled in RESORCE (Figs. 1 and 2). We show in the following that nonlinear site effects, if present, do not significantly bias the median predictions of the model.

Regarding the linear site amplification term, we consider two models, depending on the dataset (DS-EC8 or DS-VS30). The first model is $F_S = s_j C_j$, for $j = 1, \ldots 4$, where s_j are the coefficients to be determined through the regression analysis, while C_j are dummy variables used to denote the four considered EC8 site classes (A–D). The regression for the EC8 model is performed constraining to zero the coefficient for class A (reference site class). In the second model, the site effects are expressed in terms of V_{S30} as $F_S = \gamma \log_{10}(V_{S30}/V_{ref})$ where $V_{ref} = 800$ m/s and γ is to be determined through the regression.

The functional form F_{sof} in Eq. (1) represents the style of faulting correction and it is given by $F_{sof} = f_j E_j$, for $j = 1, \ldots 4$, where f_j are the coefficients to be determined during the analysis and E_j are dummy variables used to denote the different fault classes: normal (N), reverse (R), strike-slip (S) and unspecified (U). Since earthquakes with unknown style of faulting are not included in DS-VS30 the class U is considered only for DS-EC8. The reference style of faulting conditions (i.e. parameters constrained to zero in the regressions) are class U for DS-EC8 and the average over the three classes N, R, S for DS-VS30.

After trial regressions, the variables Mref, Mh, Rref (Eqs. 2 and 3) have been fixed to 5.5, 6.75 and 1 km, respectively. Coefficients c_3 and b_3 are constrained to be non-negative. As response variable Y, the geometric mean of the horizontal components for peak ground acceleration (PGA in cm/s^2) and velocity (PGV in cm/s) are considered, along with 5 % damped pseudo-spectral acceleration (PSA in cm/s^2) computed over 27 periods in the range 0.02-3 s. The regressions are performed applying a random effect approach (Abrahamson and Youngs 1992), that allows to determine the components of the standard deviation of the regression (commonly referred to as sigma, σ), namely the between-events (τ) and the within-event (ϕ) components, as well as the site-to-site component (ϕ_{S2S}) (e.g., Bindi et al. 2009, 2011b). For the definition of the components of variability, see Al Atik et al. (2010). Finally, for each period, the standard error of the distribution of the coefficients is obtained through a bootstrap analysis (Efron and Tibshirani 1994) considering 30 different bootstrap replications of the original data set, being each replication composed by the same number of data as the original set but randomly selected with repetitions.

4 Results

The regression coefficients for the two datasets, and the relevant 95 % confidence intervals, are shown in Tables 1 and 2, for Joyner-Boore distance, and in Tables 3 and 4, for hypocentral distance. The tables including the 95 % confidence intervals are reported in the Appendix (Tables 6 and 7 for R_{JB}; Tables 8 and 9 for R_{hypo}).

Table 1 Coefficients for the model derived in this study (see Eqs. 1–3) for R_{JB} and EC8 ground categories

T[~~sec~~]	0.02	0.04	0.07	0.1	0.15	0.2	0.26	0.3	0.36	0.4	0.46	0.5
e1	3.47806	3.58006	3.78163	3.7926	3.77838	3.69276	3.6761	3.66966	3.59721	3.55671	3.50177	3.45717
c1	−1.37519	−1.43327	−1.46134	−1.41441	−1.29344	−1.18195	−1.16549	−1.1752	−1.14479	−1.1452	−1.1308	−1.11631
c2	0.218095	0.238839	0.225844	0.208667	0.16355	0.119101	0.102609	0.099164	0.095008	0.094317	0.100456	0.101994
h	5.90684	5.79394	6.62019	6.89248	6.71735	5.78659	5.45192	5.40732	5.02064	5.08066	4.95777	4.69877
c3	0.00071	0.000685	0.001176	0.001602	0.002029	0.002123	0.001654	0.001248	0.000919	0.000673	0.000583	0.000509
b1	−0.02683	−0.05688	−0.04305	−0.05845	−0.03586	0.067202	0.129716	0.145499	0.168179	0.173884	0.190813	0.203522
b2	−0.0726	−0.06373	−0.04979	−0.06443	−0.09154	−0.09151	−0.09751	−0.10488	−0.11422	−0.12015	−0.12318	−0.12608
b3	0	0	0	0	0.085537	0.145251	0.135986	0.135159	0.149582	0.151849	0.130847	0.122339
ClassA	0	0	0	0	0	0	0	0	0	0	0	0
ClassB	0.134904	0.133973	0.139714	0.155236	0.158937	0.138968	0.126737	0.113881	0.109638	0.110223	0.108079	0.108783
CalssC	0.226827	0.218136	0.206862	0.210168	0.199726	0.216584	0.249141	0.259274	0.274211	0.280836	0.298022	0.305295
ClassD	0.213357	0.176183	0.145621	0.156052	0.186495	0.1995	0.229736	0.252504	0.282686	0.301657	0.34708	0.370989
sofN	−0.02809	−0.03866	−0.03889	−0.01955	−0.02056	0.018953	0.023563	0.018438	0.012675	0.02215	0.017165	0.016712
sofR	0.077532	0.060308	0.07126	0.084246	0.074269	0.133352	0.143428	0.138662	0.122472	0.129181	0.115968	0.114252
sofS	−0.02064	−0.0334	−0.02736	−0.02283	−0.02673	0.026665	0.039234	0.043489	0.036662	0.046123	0.044778	0.049822
sofU	0	0	0	0	0	0	0	0	0	0	0	0
τ	0.182533	0.18063	0.194176	0.181926	0.18138	0.177903	0.178211	0.184254	0.184085	0.191734	0.19969	0.200063
ϕ	0.278823	0.289652	0.296609	0.306918	0.305998	0.300131	0.300652	0.295463	0.295192	0.292878	0.291096	0.29164
ϕ_{S2S}	0.208393	0.220859	0.235714	0.244969	0.241833	0.219913	0.200662	0.193285	0.187569	0.180758	0.182941	0.175988
σ	0.333258	0.341358	0.354515	0.356785	0.355716	0.348896	0.349501	0.348207	0.347887	0.350056	0.353006	0.353665

Table 1 continued

T[s~~ec~~]	0.6	0.7	0.9	1	1.3	1.5	1.8	2	2.6	3	~~PGA~~	~~PGV~~
e1	3.38799	3.34381	3.25802	3.16899	3.14649	2.89515	2.76366	2.63662	2.6215	2.46318	2.3968	3.45078
c1	−1.1047	−1.11609	−1.10907	−1.08714	−1.09387	−1.03042	−1.01437	−1.04838	−1.0543	−1.07308	−1.05706	−1.36061
c2	0.104529	0.099989	0.119754	0.117879	0.114285	0.136666	0.1441	0.180838	0.181367	0.226407	0.248126	0.215873
h	4.54643	4.64017	4.63849	4.50481	4.53118	4.53208	4.61172	5.39607	5.56772	6.23491	6.7674	6.14717
c3	0.000249	0	0	0	0	0	0	0	0	0	0	0.000733
b1	0.242603	0.280922	0.291242	0.311362	0.359324	0.393471	0.432513	0.434162	0.458752	0.475305	0.48108	−0.02087
b2	−0.12601	−0.12461	−0.1226	−0.12373	−0.11774	−0.11544	−0.1043	−0.0963	−0.09558	−0.07881	−0.07197	−0.07224
b3	0.095965	0.092048	0.032748	0.052576	0.044584	0	0	0	0	0	0	0
Class A	0	0	0	0	0	0	0	0	0	0	0	0
Class B	0.106929	0.102965	0.097481	0.087057	0.086496	0.092091	0.103385	0.107251	0.099358	0.105913	0.127642	0.137715
Class C	0.321296	0.331801	0.341281	0.342803	0.34521	0.345292	0.342842	0.333706	0.329709	0.312454	0.318684	0.233048
Class D	0.440581	0.503562	0.542709	0.581633	0.590175	0.618805	0.653192	0.618956	0.604177	0.577657	0.597588	0.214227
SofN	0.013695	0.024399	0.024483	0.042376	0.053679	0.087972	0.123393	0.161886	0.139794	0.125695	0.052424	−0.03228
SofR	0.100223	0.092189	0.078739	0.091254	0.091382	0.119863	0.165217	0.193198	0.167929	0.153396	0.047119	0.073678
SofS	0.042018	0.049609	0.049226	0.068452	0.067455	0.100768	0.143638	0.201695	0.185814	0.173281	0.116645	−0.01943
SofU	0	0	0	0	0	0	0	0	0	0	0	0
τ	0.207756	0.208828	0.211136	0.220213	0.221524	0.222493	0.218105	0.212905	0.22224	0.223041	0.236576	0.180904
ϕ	0.289459	0.290952	0.294168	0.293618	0.295365	0.296657	0.303878	0.31036	0.309638	0.310755	0.302186	0.276335
ϕ	0.176453	0.178954	0.18031	0.194549	0.196091	0.196817	0.19849	0.201126	0.202676	0.20708	0.21241	0.206288
σ	0.356299	0.358137	0.362096	0.367022	0.369206	0.370822	0.374047	0.376367	0.381138	0.382513	0.383777	0.330284

Acceleration is in (cm/s^2), velocity in (cm/s). The symbols τ, ϕ, ϕ_{S2S}, and σ stand for between-events, within-event, site-to-site and total standard deviations. Sof indicates the Style of Faulting (*N* normal, *R* reverse, *S*:strike slip, *U* unknown). EC8 ground categories are indicated as Class A, B, C, D

Table 2 Coefficients for the model derived in this study (see Eqs. 1–3) for R_{JB} and Vs30 classification

T[se~~e~~]	0.02	0.04	0.07	0.1	0.15	0.2	0.26	0.3	0.36	0.4	0.46	0.5
e1	3.37053	3.43922	3.59651	3.68638	3.68632	3.68262	3.64314	3.63985	3.5748	3.53006	3.43387	3.40554
c1	−1.26358	−1.31025	−1.29051	−1.28178	−1.17697	−1.10301	−1.08527	−1.10591	−1.09955	−1.09538	−1.06586	−1.05767
c2	0.220527	0.244676	0.231878	0.219406	0.182662	0.133154	0.115603	0.108276	0.103083	0.101111	0.109066	0.112197
h	5.20082	4.91669	5.35922	6.12146	5.74154	5.31998	5.13455	5.12846	4.90557	4.95386	4.6599	4.43205
c3	0.001118	0.001092	0.001821	0.002114	0.00254	0.002421	0.001964	0.001499	0.001049	0.000851	0.000868	0.000789
b1	−0.08906	−0.11692	−0.08501	−0.11355	−0.09287	0.010086	0.02994	0.03919	0.052103	0.045846	0.060084	0.088319
b2	−0.09162	−0.07838	−0.057	−0.07533	−0.10243	−0.10518	−0.12717	−0.13858	−0.15139	−0.16209	−0.1659	−0.16411
b3	0	0	0	0	0.073904	0.150461	0.178899	0.189682	0.216011	0.224827	0.197716	0.15475
γ	−0.29402	−0.24177	−0.20763	−0.17324	−0.20249	−0.29123	−0.35443	−0.39306	−0.45391	−0.49206	−0.56446	−0.5962
sofN	−0.03924	−0.03772	−0.04594	−0.03805	−0.02673	−0.03265	−0.03384	−0.03725	−0.02791	−0.02563	−0.01866	−0.01742
sofR	0.081052	0.079778	0.087497	0.08471	0.067844	0.075977	0.074982	0.076701	0.06979	0.072567	0.064599	0.060283
sofS	−0.04182	−0.04206	−0.04155	−0.04666	−0.04111	−0.04332	−0.04114	−0.03946	−0.04188	−0.04694	−0.04594	−0.04286
τ	0.15867	0.154621	0.172785	0.169691	0.152902	0.150055	0.151209	0.157946	0.165436	0.157728	0.173005	0.18082
ϕ	0.282356	0.291143	0.291499	0.301967	0.305804	0.300109	0.302419	0.297402	0.294395	0.296992	0.291868	0.289957
ϕ_{S2S}	0.183959	0.187409	0.199913	0.208178	0.212124	0.190469	0.187037	0.174118	0.175848	0.169883	0.164162	0.16509
σ	0.323885	0.329654	0.33886	0.346379	0.3419	0.335532	0.338114	0.336741	0.337694	0.336278	0.33929	0.341717

Table 2 continued

T[s~~ec~~]	0.6	0.7	0.9	1	1.3	1.5	1.8	2	2.6	3	~~PGA~~	~~PGV~~
e1	3.30442	3.23882	3.1537	3.13481	3.12474	2.89841	2.84727	2.68016	2.60171	2.39067	2.25399	3.32819
c1	−1.05014	−1.05021	−1.04654	−1.04612	−1.0527	−0.97383	−0.98339	−0.98308	−0.97922	−0.97753	−0.94037	−1.2398
c2	0.121734	0.114674	0.129522	0.114536	0.103471	0.104898	0.109072	0.164027	0.163344	0.211831	0.227241	0.21732
h	4.21657	4.17127	4.20016	4.48003	4.41613	4.25821	4.56697	4.68008	4.58186	5.39517	5.74173	5.26486
c3	0.000487	0.000159	0	0	0	0	0	0	0	0	0	0.001186
b1	0.120182	0.166933	0.193817	0.247547	0.306569	0.349119	0.384546	0.343663	0.331747	0.357514	0.385526	−0.0855
b2	−0.16333	−0.16111	−0.15655	−0.15382	−0.14756	−0.14948	−0.13987	−0.13593	−0.14828	−0.12254	−0.11145	−0.09256
b3	0.117576	0.112005	0.051729	0.081575	0.092837	0.108209	0.098737	0	0	0	0	0
γ	−0.66782	−0.73839	−0.79408	−0.8217	−0.82658	−0.84505	−0.8232	−0.77866	−0.76924	−0.76961	−0.73207	−0.3019
SofN	−0.00049	0.011203	0.016526	0.016449	0.026307	0.025234	0.018674	0.011371	0.005535	0.008735	0.022989	−0.03977
SofR	0.044921	0.028151	0.020352	0.021242	0.018604	0.022362	0.023089	0.016688	0.019857	0.023314	−0.02066	0.077525
SofS	−0.04443	−0.03935	−0.03688	−0.03769	−0.04491	−0.0476	−0.04176	−0.02806	−0.02539	−0.03205	−0.00233	−0.03776
τ	0.182233	0.189396	0.189074	0.191986	0.195026	0.181782	0.177752	0.163242	0.164958	0.17028	0.176546	0.149977
ϕ	0.292223	0.289307	0.288815	0.293264	0.297907	0.306676	0.316312	0.326484	0.329916	0.320626	0.314165	0.282398
ϕ	0.175634	0.168617	0.16817	0.183719	0.200775	0.209625	0.218569	0.221367	0.22535	0.210193	0.207247	0.165611
σ	0.344388	0.345788	0.3452	0.350517	0.356067	0.356504	0.362835	0.36502	0.368857	0.363037	0.360373	0.319753

Acceleration is in (cm/s^2), velocity in (cm/s). The symbols τ, ϕ, ϕ_{S2S}, and σ stand for between-events, within-event, site-to-site and total standard deviations. Sof indicates the Style of Faulting (*N* normal, *R* reverse, *S* strike slip). The site coefficient is indicated as γ

Table 3 Coefficients for the model derived in this study (see Eqs. 1–3) for R_{HYPO} and EC8 ground categories

T[se~~e~~]	0.02	0.04	0.07	0.1	0.15	0.2	0.26	0.3	0.36	0.4	0.46	0.5
e1	4.42044	4.54992	4.73285	4.67503	4.56965	4.45017	4.45593	4.47171	4.38799	4.37609	4.33372	4.29359
c1	−1.77754	−1.8546	−1.87822	−1.79917	−1.61405	−1.46501	−1.44342	−1.46016	−1.41842	−1.42843	−1.42503	−1.41465
c2	0.147715	0.165968	0.157048	0.151808	0.105601	0.056755	0.032061	0.025927	0.02215	0.016902	0.025903	0.028368
h	7.06428	6.98227	8.1337	8.38098	7.49625	6.27222	5.4804	5.50316	4.76952	4.81974	5.10961	4.95519
c3	0	0	0	0.000548	0.001183	0.001431	0.000982	0.000554	0.000269	0	0	0
b1	0.147874	0.124402	0.138028	0.098832	0.125747	0.236642	0.313239	0.332549	0.355357	0.368987	0.379142	0.38941
b2	−0.06621	−0.0566	−0.04079	−0.05694	−0.0835	−0.08346	−0.08972	−0.09722	−0.10604	−0.11196	−0.11515	−0.11815
b3	0.29709	0.260601	0.27609	0.322027	0.464456	0.542025	0.555789	0.551296	0.543724	0.547881	0.511833	0.495459
Class A	0	0	0	0	0	0	0	0	0	0	0	0
Class B	0.14111	0.14035	0.145543	0.158622	0.162534	0.143446	0.133443	0.121637	0.118062	0.119481	0.117659	0.118871
CalssC	0.225339	0.21701	0.206101	0.208849	0.197589	0.213637	0.244854	0.254554	0.268087	0.275041	0.291964	0.29887
Class D	0.187033	0.146507	0.115846	0.125428	0.158161	0.170195	0.202162	0.226009	0.258058	0.275672	0.321124	0.344584
sofN	−0.06531	−0.06538	−0.05129	−0.03749	−0.04709	−0.02145	−0.03049	−0.04227	−0.05667	−0.05327	−0.06251	−0.06474
sofR	0.091732	0.088098	0.113143	0.120065	0.098046	0.139454	0.132769	0.119803	0.092863	0.09198	0.073772	0.069449
sofS	−0.05613	−0.05767	−0.03762	−0.0369	−0.05061	−0.01246	−0.01516	−0.01923	−0.03496	−0.03219	−0.03929	−0.03741
sofU	0	0	0	0	0	0	0	0	0	0	0	0
τ	0.197407	0.204345	0.208843	0.19539	0.193856	0.191231	0.192222	0.199096	0.199491	0.207716	0.216313	0.225415
ϕ	0.287767	0.297881	0.304438	0.31332	0.310861	0.306652	0.308241	0.304125	0.304728	0.302796	0.30138	0.300553
ϕ_{S2S}	0.216309	0.222929	0.242821	0.251339	0.247987	0.226544	0.214042	0.207111	0.201784	0.194828	0.197633	0.198934
σ	0.348969	0.361234	0.369185	0.369252	0.366353	0.361392	0.363266	0.363499	0.36422	0.367194	0.370974	0.375691

Table 3 continued

T[~~sec~~]	0.6	0.7	0.9	1	1.3	1.5	1.8	2	2.6	3	~~PGA~~	~~PGV~~
e1	4.23915	4.19696	4.11453	4.03249	4.0114	3.68402	3.53587	3.46588	3.4691	3.28384	3.2647	4.36693
c1	−1.40603	−1.41297	−1.40429	−1.38977	−1.39543	−1.30231	−1.27351	−1.36102	−1.38111	−1.38977	−1.39974	−1.75212
c2	0.02698	0.020876	0.038146	0.037094	0.034061	0.069535	0.082246	0.137018	0.137878	0.188643	0.216533	0.150507
h	4.63597	4.29377	4.01059	3.97812	4.09668	3.7329	4.07408	6.0971	6.53917	7.04011	8.33921	7.32192
c3	0	0	0	0	0	0	0	0	0	0	0	0
b1	0.430341	0.470648	0.481962	0.504043	0.550001	0.544404	0.570581	0.524014	0.551312	0.547984	0.552993	0.144291
b2	−0.11928	−0.1181	−0.11674	−0.11665	−0.11086	−0.11362	−0.10376	−0.10109	−0.09877	−0.08423	−0.07134	−0.06608
b3	0.475308	0.460014	0.393948	0.400442	0.386023	0.282169	0.24976	0.046975	0	0	0	0.284211
Class A	0	0	0	0	0	0	0	0	0	0	0	0
Class B	0.117717	0.115734	0.110981	0.103765	0.103026	0.108865	0.119032	0.123814	0.115091	0.124833	0.143969	0.143778
Class C	0.314097	0.325887	0.334461	0.334934	0.336196	0.337519	0.33311	0.323505	0.320404	0.306133	0.315187	0.231064
Class D	0.412316	0.477053	0.51753	0.559004	0.566463	0.592894	0.626267	0.60053	0.586654	0.548523	0.559213	0.187402
SofN	−0.07608	−0.07496	−0.08163	−0.06429	−0.05717	−0.03466	−0.01067	−0.00297	−0.0238	−0.05066	−0.14667	−0.07175
SofR	0.045871	0.028575	0.008429	0.019498	0.014893	0.029824	0.060267	0.058459	0.034964	0.003435	−0.12866	0.084958
SofS	−0.05488	−0.05564	−0.06343	−0.04562	−0.05139	−0.02508	0.007386	0.039471	0.02527	0.007396	−0.06757	−0.0571
SofU	0	0	0	0	0	0	0	0	0	0	0	0
τ	0.234484	0.246498	0.249844	0.261433	0.274446	0.26531	0.269363	0.27539	0.277179	0.278908	0.283885	0.195249
ϕ	0.299514	0.301897	0.305995	0.30722	0.309616	0.311777	0.316539	0.323622	0.325724	0.327756	0.320266	0.284622
ϕ_{S2S}	0.208675	0.212696	0.224068	0.240384	0.244465	0.244067	0.236824	0.257636	0.259839	0.263531	0.267078	0.213455
σ	0.380383	0.389747	0.395038	0.403399	0.413742	0.409383	0.415637	0.424936	0.427696	0.430364	0.427973	0.345155

Acceleration is in (cm/s^2), velocity in (cm/s). The symbols τ, ϕ, ϕ_{S2S}, and σ stand for between-events, within-event, site-to-site and total standard deviations

Table 4 Coefficients for the model derived in this study (see Eqs. 1–3) for R_{HYPO} and Vs30 classification

T[sec]	0.02	0.04	0.07	0.1	0.15	0.2	0.26	0.3	0.36	0.4	0.46	0.5
e1	4.3397	4.46839	4.5724	4.55255	4.51119	4.49571	4.49224	4.51726	4.46559	4.46834	4.3715	4.34198
c1	−1.60402	−1.68536	−1.63863	−1.57947	−1.4471	−1.37039	−1.36679	−1.40078	−1.40973	−1.42893	−1.40655	−1.39751
c2	0.103401	0.126703	0.123954	0.125609	0.08461	0.038536	0.012937	0.00198	0.000489	−0.0091	0.00101	0.004238
h	4.47852	4.58063	5.12096	5.67511	4.8248	4.56965	3.94802	4.26816	4.39978	4.6039	4.60254	4.43045
c3	$2.63E{-05}$	0	0.000722	0.001239	0.001692	0.001586	0.001059	0.000565	$5.97E{-05}$	0	0	0
b1	0.230422	0.205651	0.226272	0.167382	0.194714	0.289627	0.321065	0.336096	0.346351	0.353351	0.35717	0.384532
b2	−0.06654	−0.05281	−0.0298	−0.05091	−0.07845	−0.08155	−0.10418	−0.11526	−0.12711	−0.13778	−0.14277	−0.14092
b3	0.363906	0.323734	0.311109	0.348968	0.448903	0.533244	0.596455	0.612107	0.600314	0.621323	0.589127	0.543301
γ	−0.286524	−0.232462	−0.195629	−0.168432	−0.194539	−0.270912	−0.323555	−0.363199	−0.430464	−0.467397	−0.531694	−0.555531
sofN	−0.04692	−0.04517	−0.05321	−0.04704	−0.03631	−0.03868	−0.03658	−0.03807	−0.02853	−0.02616	−0.01928	−0.01758
sofR	0.115063	0.114597	0.121653	0.119021	0.102481	0.107555	0.103236	0.104818	0.095509	0.097198	0.090202	0.086012
sofS	−0.06814	−0.06943	−0.06845	−0.07198	−0.06617	−0.06888	−0.06666	−0.06675	−0.06697	−0.07104	−0.07092	−0.06843
τ	0.154538	0.158402	0.169775	0.165148	0.145533	0.144701	0.156869	0.165195	0.164907	0.165146	0.181401	0.189686
ϕ	0.290986	0.298261	0.302117	0.310963	0.310621	0.308845	0.313737	0.311052	0.310509	0.310959	0.306033	0.304174
ϕ_{S2S}	0.18825	0.192664	0.205229	0.212643	0.216313	0.20204	0.199484	0.186722	0.180734	0.182064	0.176797	0.178065
σ	0.329477	0.337714	0.346552	0.352097	0.343023	0.341063	0.350769	0.352197	0.351583	0.352092	0.355756	0.358473

Table 4 continued

T[~~sec~~]	0.6	0.7	0.9	1	1.3	1.5	1.8	2	2.6	3	~~PGA~~	~~PGV~~
e1	−1.37164	4.14832	4.09246	4.08324	4.07207	3.77954	3.69447	3.45408	3.38901	3.06601	2.89391	4.27391
c1	17.7584	−1.37169	−1.37736	−1.38649	−1.38735	−1.27343	−1.26477	−1.27364	−1.28283	−1.23427	−1.16461	−1.57821
c2	0.216704	0.002264	0.008956	−0.00453	−0.01855	−0.01377	−0.00337	0.083746	0.086724	0.150146	0.162354	0.108218
h	886.652	3.00978	3.15727	3.4537	3.3163	3.04976	3.65482	4.59988	4.95285	4.45511	4.62321	4.82743
c3	0.05606	0	0	0	0	0	0	0	0	0	0	9.64E−05
b1	−0.25583	0.466754	0.510102	0.567727	0.631338	0.650829	0.6746	0.563304	0.548353	0.54175	0.590765	0.217109
b2	−0.12108	−0.13807	−0.13263	−0.12724	−0.12124	−0.12901	−0.11908	−0.1178	−0.12957	−0.1037	−0.08533	−0.06826
b3	0	0.498126	0.437529	0.45811	0.474982	0.488244	0.461122	0.184126	0.171017	0.009303	0.034058	0.352976
γ	−0.457888	−0.698998	−0.757522	−0.786632	−0.791438	−0.803656	−0.780198	−0.749008	−0.744073	−0.744468	−0.693999	−0.293242
SofN	0.022367	0.010003	0.015018	0.01638	0.026396	0.024922	0.019123	0.011676	0.004993	0.006027	0.018621	−0.04721
SofR	0.125552	0.054388	0.045865	0.044224	0.041137	0.038329	0.038697	0.029249	0.033587	0.030508	−0.01898	0.110979
SofS	−0.14793	−0.06439	−0.06088	−0.0606	−0.06753	−0.06325	−0.05782	−0.04092	−0.03858	−0.03653	0.000361	−0.06376
τ	0.259955	0.20181	0.211664	0.225279	0.238973	0.212162	0.208441	0.203238	0.205751	0.190711	0.183363	0.145783
ϕ	0.397088	0.30827	0.30855	0.313873	0.318631	0.324083	0.33425	0.342873	0.347114	0.339373	0.326297	0.291566
ϕ_{S2S}	0.189183	0.264361	0.208994	0.225906	0.246861	0.245588	0.24415	0.256308	0.26183	0.242015	0.22865	0.186662
σ	0.474611	0.368453	0.374172	0.386351	0.398289	0.387354	0.393917	0.398582	0.403511	0.389288	0.374289	0.325981

Acceleration is in (cm/s^2), velocity in (cm/s). The symbols τ, ϕ, ϕ_{S2S}, and σ stand for between-events, within-event, site-to-site and total standard deviations

4.1 Influence of the dataset

Figures 4a, b show the comparison between ground-motion predictions obtained with the DS-EC8 or the DS-VS30 datasets. In particular, Fig. 4a exemplifies the comparison for class B of EC8, which is sampled by stations belonging to different countries (Fig. 2) and considering V_S~~$_{30}$~~ = 580 m/s. No significant differences can be appreciated both for the median and the total standard deviation.

Figure 4b shows the dependence on period of the total (σ), between-events (τ), within-event (ϕ) and site-to-site (ϕ_{S2S}) standard deviations, for the two data sets. For DS-EC8, sigma increases from 0.33 at 0.02 s to 0.38 at 3 s, while only a modest reduction of sigma is observed when DS-VS30 is considered (sigma ranges from 0.32 to 0.36 at 0.02 and 3 s, respectively), although DS-VS30 includes waveforms from stations characterized by measured Vs30. To investigate the reasons of such limited improvement, Fig. 4b also compares the other components of variability. The between-events component τ, obtained for DS-VS30, is smaller than 0.2 over the analyzed period range, while, for DS-EC8, τ is lower than 0.2 only for periods shorter than 0.5 s. The within-event component ϕ is significantly larger than τ and similar for the two data sets, except for periods longer than 1 s, where ϕ associated to DS-EC8 is smaller than the one associated to DS-VS30. This feature can be ascribed to the site-to-site standard deviation (ϕ_{S2S}). In fact, the ϕ_{S2S} evaluated using a continuous function of Vs30 is smaller than the one obtained from EC8 site categories in the short periods range (< 1 s) while, for periods longer than 1 s, it assumes larger values. Since stations belonging to EC8 classes C and D usually exhibit large amplification above 1 s, the increase of ϕ_{S2S} at long periods suggests that Vs30 is not a good proxy to capture the site effects for soft sites included in RESORCE.

4.2 Influence of distance metrics

In Fig. 5 the influence of the use of hypocentral or Joyner-Boore distances is shown for Mw 7.5 and 4, and considering EC8 class A. The two magnitudes correspond to the limits of applicability of the model. The comparison is performed for PGA and PSA at 1 s. The two models predict similar values for low magnitudes (Mw = 4) at all distances. Since the point source approximation can be applied, for small magnitudes R_{JB} is similar to the epicentral distance and the difference between R_{JB} and R_{hypo} is related to the focal depth. For short distances and large magnitudes the model based on R_{hypo} predicts larger values than the one based on R~~$_{JB}$~~, as the difference in the definition of the two metrics, can cause R_{JB} close to zero, even for considerable epicentral (and hence hypocentral) distances.~~,~~

In the following, since the models based on DS-EC8 or DS-VS30 are similar in terms of median predictions and standard deviation, we limit the discussion to the DS-EC8 dataset and the Joyner-Boore distance.

4.3 Coefficients of GMPEs

Figure 6 shows that nearly all coefficients have a significant dependence on period. The coefficient b_3, controlling the magnitude-dependence over the hinge-magnitude, is positive in the period range 0.15–1.5 s, although these values are not significantly different from zero at a 5 % significance level. The coefficient c_3, relative to the linear attenuation with distance is significantly different from zero, at a 5 % significance level only for $0.04 < T < 0.4$ s. The pseudo-depth parameter h varies from 4.5 to 6.9 km, with an average of 5.5 km.

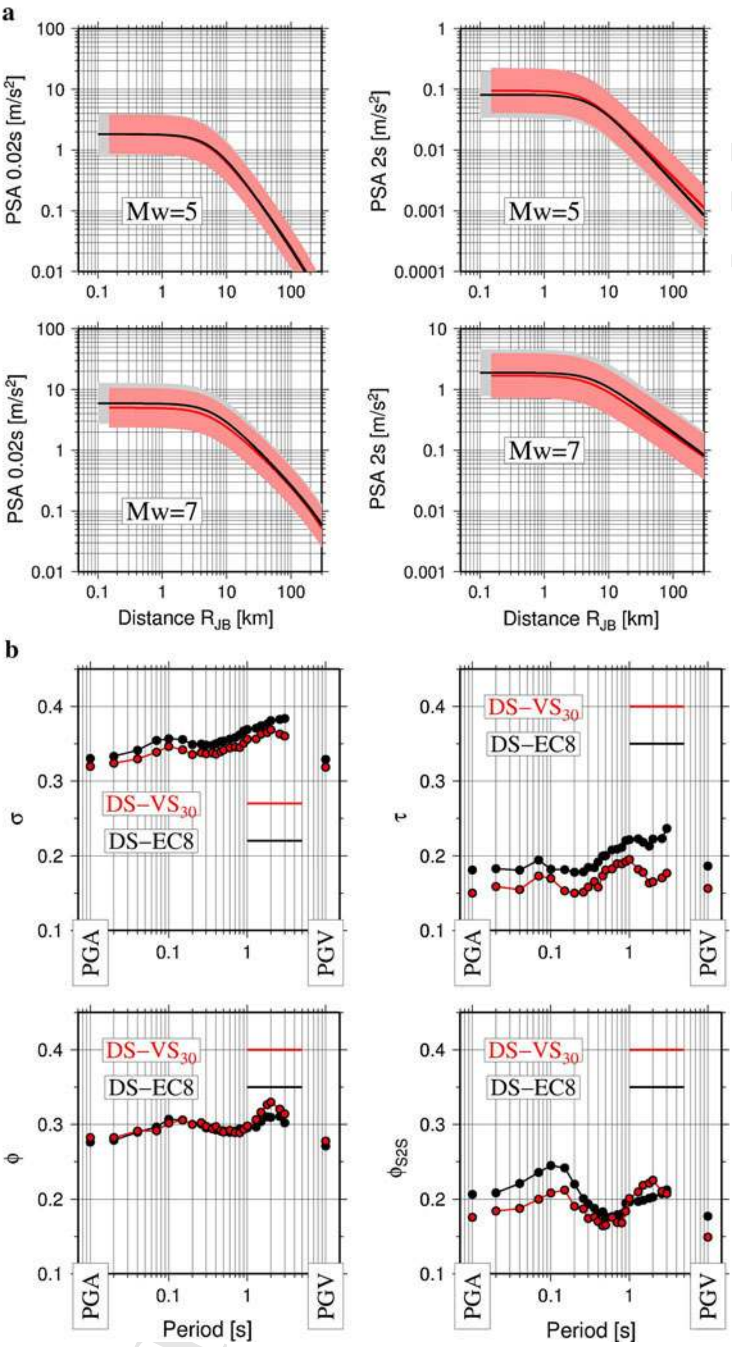

Fig. 4 **a** Comparisons between the ground motion predictions obtained with the two datasets (*red color* is DS-V~~s30~~ and *grey color* is DS-EC8). *Left panel* T = 0.02 s, *right panel* T = 2 s. The *curves* are relative to normal fault and Ec8 class B (Vs30 = 580 m/s). **b**. Standard deviations obtained for the two datasets (*top left*: total sigma; *top right*: between-events standard deviation; *bottom left*: within-event standard deviation; *bottom right*: site-to-site standard deviation)

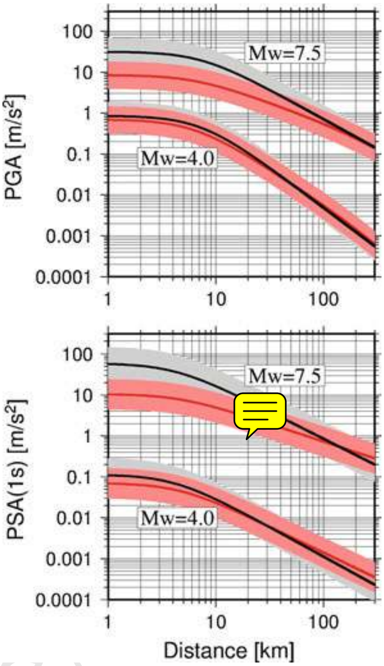

Fig. 5 Comparison between models based on Joyner-Boore (*red*) or hypocentral distances (*grey scale*) for PGA (~~*upper*~~ *panel*) and PSA at T = 1 s (~~*lower*~~ *panel*) for DS-EC8 dataset, considering class C and strike slip faulting

The site coefficients are shown in Fig. 7. Site category B (i.e. stiff sites) amplifies the entire period range with values between 0.10 and 0.15 log10 units; class C shows an almost constant amplification of about 0.21, for periods up to 0.2 s, and a peak of amplification of about 0.34 at 1 s; class D has a relevant amplification (up to 0.62) for periods longer than 1 s. Class D is represented by 31 stations but only 5 are characterized by at least 5 recordings, namely: Bevagna (BVG, Italian station with 7 records analyzed in this study at 1 s); Colfiorito (CLF, Italy, 14 records at 1 s); Norcia (NOR, Italy, 5 records at 1 s); Rieti (RTI, Italy, 7 records); Ambarli (ATS, Turkey, 6 records). Therefore, the above mentioned stations strongly control the amplification coefficient of the entire class (Bindi et al. 2011b). In fact, the amplification peak of class D (Fig. 7) reflects the long period (> 1 s) site amplifications found by Rovelli et al. (2001) for CLF; Bindi et al. (2011c) for station NOR; Foti et al. (2011), for RTI; Luzi et al. (2005) for BVG. Figure 7 also shows the style of faulting coefficients, indicating that reverse faulting causes amplitudes higher than strike-slip and normal faulting, at short periods (0–1 s), while normal and strike slip coefficients show similar trend.

Regarding the propagation of errors from data to solutions, Fig. 8 (top panel) exemplifies the unit covariance matrix (Menke 1989), computed for T = 0.1 s. The parameters most affected by the amplification of error from data to solutions are e_1, h and b_3 (i.e., those having the largest diagonal elements), that also show significant trade-offs with the other parameters. These results are in agreement with the data distribution shown in Fig. 1, relative to the sparse sampling at short distances (controlling e_1 and h) and large magnitudes (controlling b_3). Figure 6 (top panel) illustrates the trade-off of coefficients e_1 (C_{1j} elements) and h (C_{4j} elements). The off-set coefficient e_1 shows positive trade-off with pseudo-depth h ($C_{14} = 0.597$ at $T = 0.1$ s), with b_3($C_{16} = 0.036$) and negative trade-off with c_1($C_{12} = -0.0597$), which, in turn, shows a negative trade-off with the pseudo-depth parameter ($C_{42} = -0.434$).

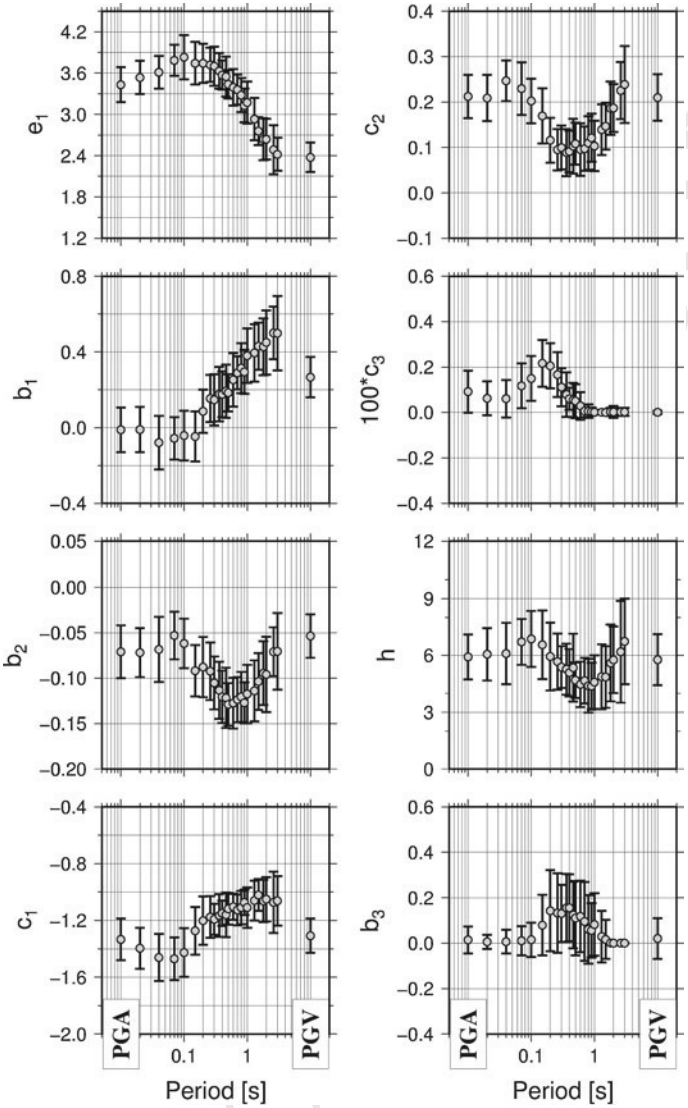

Fig. 6 Mean and 95 % confidence interval versus period of the coefficients relevant to the model described in Eqs. 1–3 (DS-EC8 data set). PGA is reported at T = 0.01 s (first point the left), while the Peak Ground Velocity (PGV) at T = 10 s (last point on the right)

The constraint applied to the site amplification for class A removes the trade-off between the offset coefficient e_1 and the site coefficients while a weak trade-off among the style of faulting coefficients and e_1 still persists. Finally, all the entries of the covariance matrix show a weak-dependence on period (Fig. 8 middle and bottom panels) although C_{14} and C_{44}, have a sharp increase for periods longer than 1 s. At long periods, the trade-off between the pseudo-depth parameter h and the off-set parameter e_1 (C_{14}) increases and h is poorly constrained (C_{44}). An explanation for the increase of this trade-off could be the decreasing number of recordings due to the filter selection (Fig. 3).

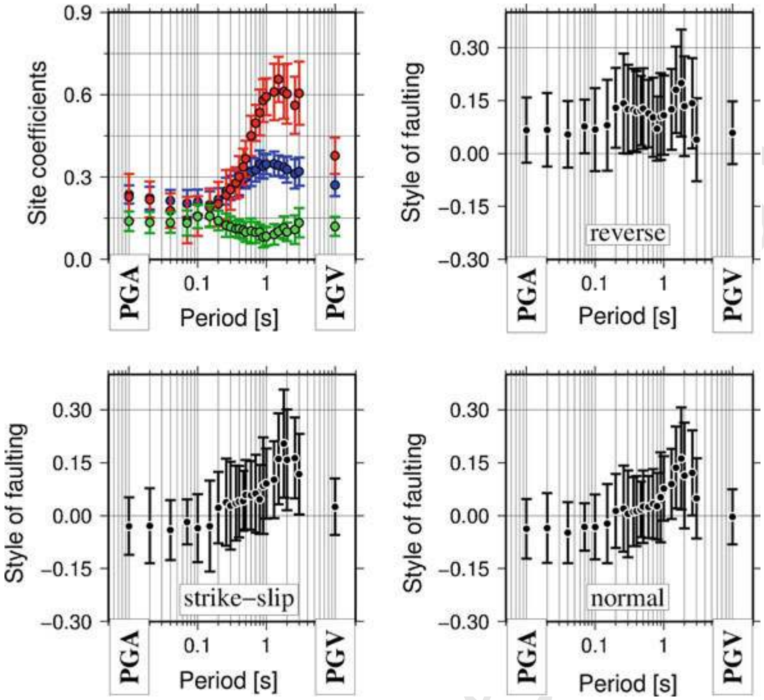

Fig. 7 *Top Left*: Site coefficients for EC8 classes B through D versus period (*green*: class B; *blue*: class C; *red*: class D). *Top Right*: Style-of-faulting coefficients versus period for reverse faulting. *Bottom*: style of faulting for strike slip (*left*) and normal (*right*) faulting. Peak Ground Acceleration (PGA) is reported at T = 0.01 s (first point the left), while the Peak Ground Velocity (PGV) at T = 10 s (last point on the right)

5 Ground-motion variability

We carry out the residuals analysis with the aim of investigating the possible origins of uncertainties not captured by the GMPEs, and to check for any dependence on the primary explanatory variables. Figure 9 shows, at fixed periods of 0.02 s (left panels) and 2.0 s (right panels): (i) the residuals (log10 of the observed—predicted values), (ii) the between-events errors in function of magnitude (second row), (iii) the site-to-site errors in function of the EC8 ground categories (third row) and (iv) the record-to-record errors (that is, the residuals corrected for the between-events and site-to-site errors) in function of R_{JB} distance (fourth row).

To investigate the influence of the earthquake type on the predicted ground-motion, the total residuals (Fig. 9, first row) relative to aftershocks and mainshocks are displayed with different colors. Since it is difficult to find objective criteria to separate mainshocks and aftershocks in the European datasets (see also Douglas and Halldórsson 2010), we apply the Gardner and Knopoff (1974) approach, and we exploit the information available in the metadata. The histograms of the residuals for aftershocks and mainshocks are shown in Fig. 10 (top panels), indicating that the distributions are almost unbiased for both type of earthquakes, and the normal distributions that best fit the histograms have nearly the same sigma (e.g., 0.369 and 0.364 for mainshocks and afterschocks, respectively, at T = 2 s). Considering the between-events errors distribution (bottom panels of Fig. 10), a slightly smaller standard

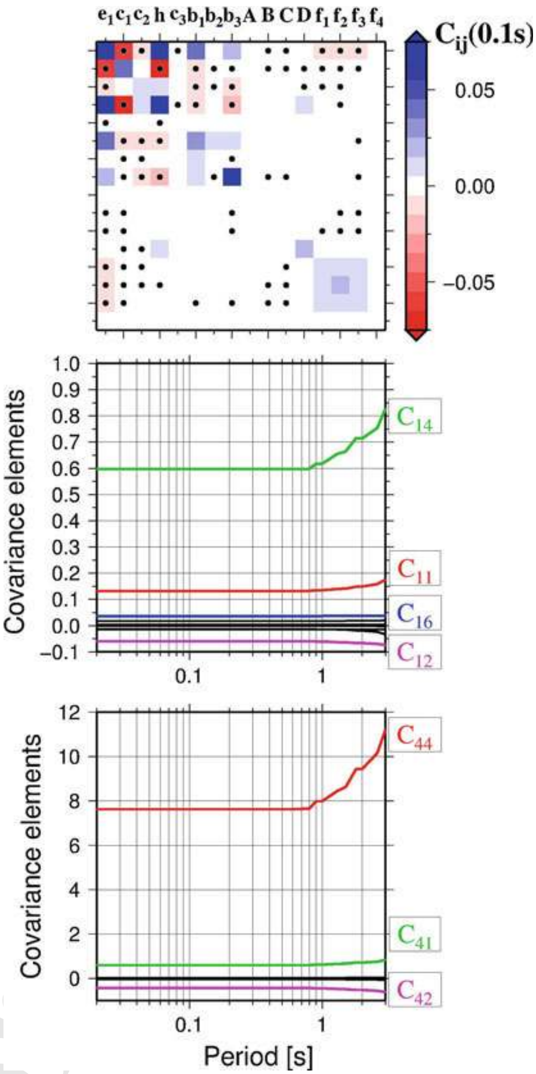

Fig. 8 *Top panel*: unit covariance matrix computed for the final model at T = 0.1 s (*blue*: positive entries, *red*: negative entries; *black dots* also indicate negative entries). *Middle panel*: entries in the columns of the covariance matrix relevant to the parameter e_1 (first row or first column) against period. *Bottom panel*: entries in the columns of the covariance matrix relevant to the parameter h (fourth row or fourth column)

deviation is observed for the mainshock distribution with respect to the aftershock one (0.169 against 0.181 at 2 s; 0.130 against 0.154 at 0.02 s) together with slightly larger bias for mainshocks (0.0332 against 0.0147 at 2 s). The small differences in the statistical parameters of the normal distributions shown in Fig. 10 suggest that neglecting the classification of the earthquake type in the predictive model, introduces a negligible bias in the residuals, with a weak tendency of underestimating the ground-motion at long periods for mainshocks.

The plot of the between-events errors in function of magnitude (Fig. 9, second row), shows an increase of dispersion for small magnitude and long periods, although the low dispersion at large magnitude could be an apparent effect related to the poor sampling. The large positive between-events error at T = 2 s is relevant to Mw 6.2, 2004 Baladeh (Iran) earthquake (e.g., Tatar et al. 2007; Ghasemi et al. 2008), whose processing over long periods should be revised. The top panel of Fig. 11 presents the between-events standard deviation τ computed grouping

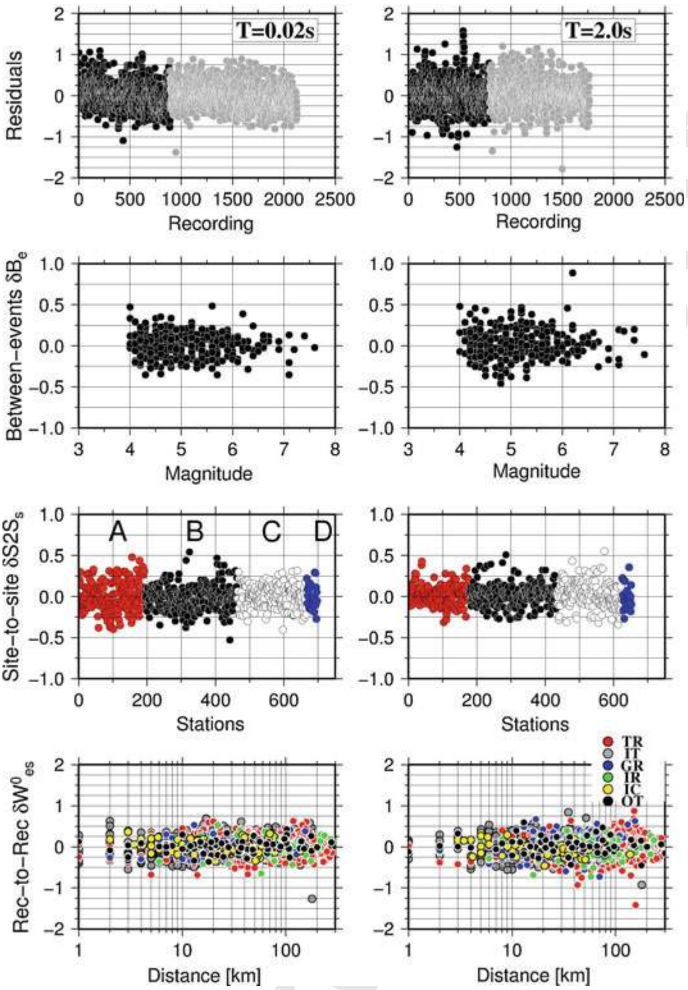

Fig. 9 *Left panels* are T = 0.02 s and *right panels* are T = 2.0 s. *First row*: distribution of residuals (computed as $\log_{10}$ of observations over predictions), where the *black* and *gray dots* indicate mainshocks and aftershocks, respectively; *second row*: between-events residuals in function of magnitude; *third row*: site-to-site residuals (*red*: class A *black*: class B *white*: class C *blue*: class D); *fourth row*: record-to-record residuals (the colours indicate different recording networks)

the earthquakes into three magnitude ranges ($M \leq 5$; $5 < M \leq 6$; $M > 6$), without considering the Baladeh earthquake. While the standard deviations are almost the same for short period ($T < 0.2$ s), at longer periods ($T > 1$s) τ is significantly larger for small magnitudes ($M < 5$), with respect to the well sampled magnitude range $5 < M < 6$. The dependence of τ on magnitude suggests that a heteroscedastic model, including a magnitude dependent sigma, should be considered in deriving GMPEs, although it would be necessary an increase of sampling of large earthquakes.

The site-to-site errors are shown according to their EC8 site classes (Fig. 9, third row). A larger dispersion of class A at short periods and of classes B and C at long periods is observed. This trend is analyzed in detail in the middle panel of Fig. 11, where the standard deviation

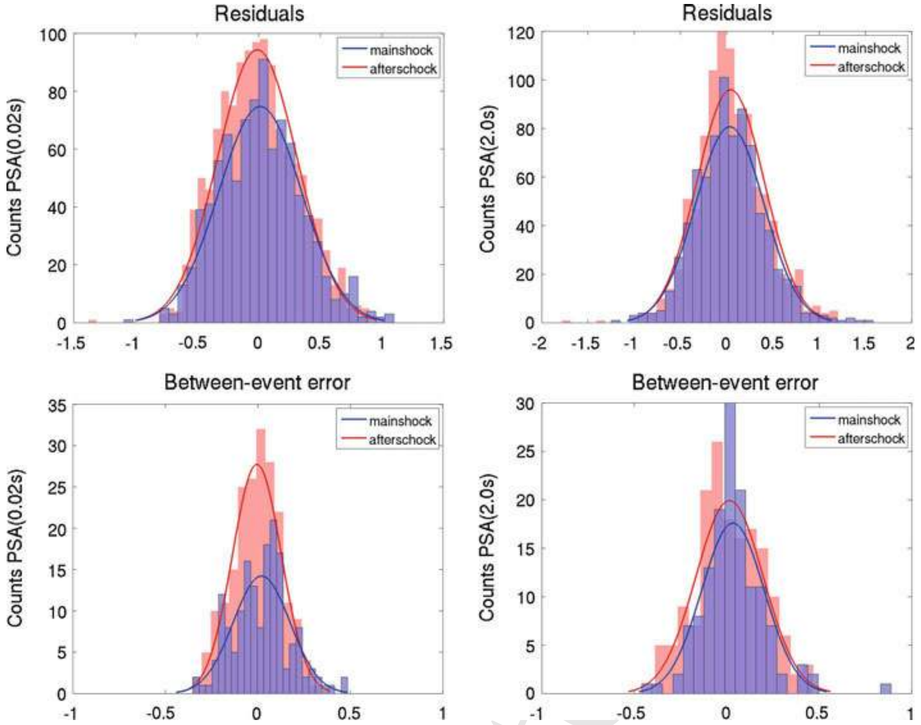

Fig. 10 *Top*: Histograms of the total residual at T = 0.02 s (*left*) and at T = 2 s (*right*) and best fit Gaussian models. *Bottom*: the same as in the top panels but for the between-events residuals. *Red bars* and *curves*: aftershocks; *blue bars* and *curves*: mainshocks. Please note the different scales on the axes

ϕ_{S2S} of the site-to-site error is computed separately for the four different site categories. For all classes, ϕ_{S2S} assumes the largest value around 0.1 s and the minimum around 0.5 s. For $T < 0.2$ s, the largest ϕ_{S2S} are those relevant to classes A and B while, for $T > 1$ s, the largest values are obtained for classes C and D.

The record-to-record errors are shown in the bottom panels of Fig. 9, grouped according to the recording network. The histograms computed for each country are shown in Fig. 12. For T = 0.2 s, the distributions for the different networks have zero mean and similar standard deviations. For T = 2 s, small differences among the mean record-to-record error for different networks are observed. Greece and Turkey shows the largest standard deviation (0.26 and 0.24, respectively), while the standard deviation for Iran, Italy and Iceland are 0.23, 0.20 and 0.15, respectively.

To investigate the presence of possible biases in the residual distributions due to non linear site effects not modeled in the GMPEs, Fig. 13 shows the record-to-record distribution of errors for PGA and PGV versus Vs30 (top panels) and the observed peak values (bottom panels). The error distributions do not show any trend with Vs30, while a weak positive trend is observed with respect to the input values. This trend is opposite to the one expected in case of non-linear site effects. Moreover, the trend is the same for soft ($Vs30 < 360$ m/s) and stiff/rock ($Vs30 > 30$ m/s) sites. We conclude that non-linear site effects are not leaving a significant imprint in the residuals with respect the predictions from a model including only a linear site term.

Fig. 11 ~~*Top*~~: Between-events standard deviation τ compute for three different magnitude classes; ~~*Bottom*~~: site-to-site standard deviation ϕ_{S2S} computed for the 4 considered EC8 site classes

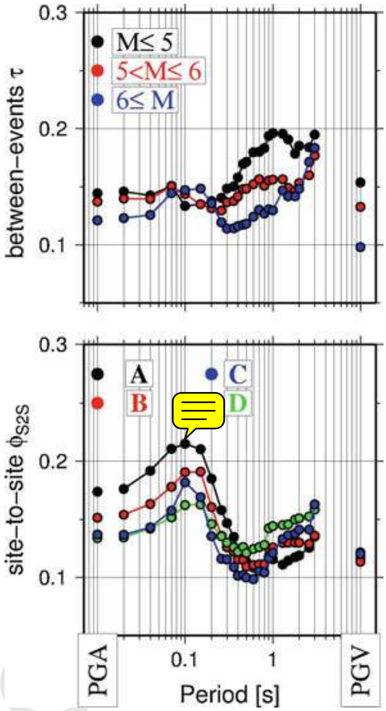

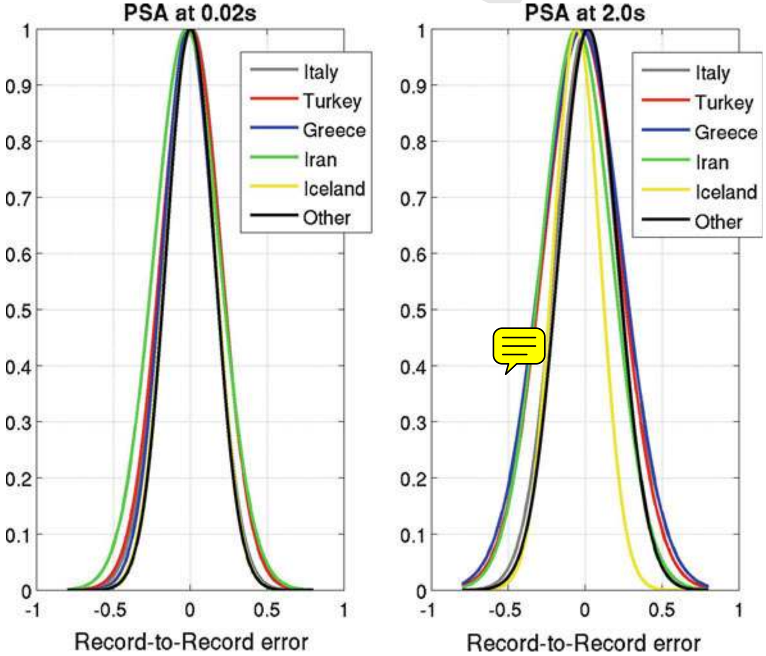

Fig. 12 Record-to-record residuals at T = 0.02 s (*left*) and at T = 2 s (*right*). The *colors* are relative to the different networks as indicated in the legend

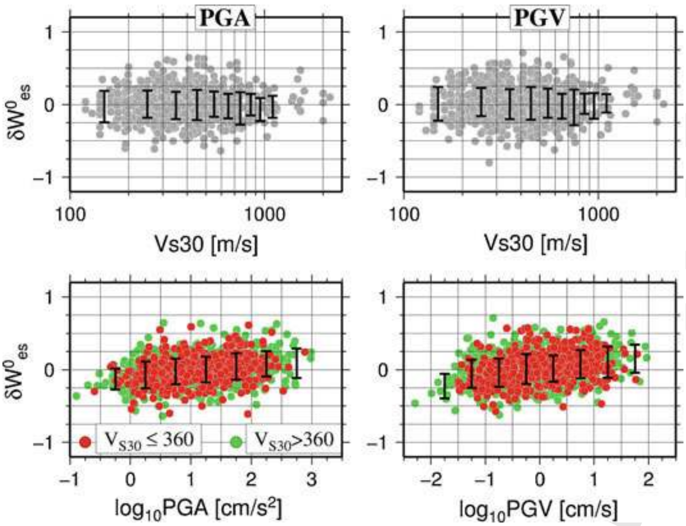

Fig. 13 *Top*: Record-to-record δW^0_{se} errors versus Vs30 for PGA (*left*) and PGV (*right*). Mean ± one standard deviation values (*vertical bars*) are computed over velocity bins 100 m/s wide except than the *first vertical bar*, computed over the range Vs30 $<$ 200 m/s^2, and the last over the range Vs30 $>$ 1000 m/s^2. *Bottom*. Record-to-record δW^0_{se} errors versus log$_{10}$ PGA (*left*) and log$_{10}$PGV (*right*). *Red* and *green filled circles* correspond to recordings at site with Vs30 $\leq$ 360 m/s^2 and Vs30 $>$ 360m/s^2, respectively

6 Comparison with NGA and regional models

We compare the equations derived in this study to both global (Akkar and Bommer 2010, AB10; Cauzzi and Faccioli 2008, CF08; NGA equations by Boore and Atkinson 2008, BA08; Campbell and Bozorgnia 2008, CB08) and regional GMPEs (Bindi et al. 2011a, ITA10, developed for Italy; Akkar and Cagnan 2010, AC10, developed for Turkey; Danciu and Tselentis 2007, DT07, developed for Greece). The main characteristics of these GMPEs are listed in Table 5. For the BA08 model, the correction factors for small magnitudes proposed by Atkinson and Boore (2011) are applied. As the GMPEs are based on different distance metrics, the hypocentral distances, used by CF08, have been converted into R_{JB} using the relationships proposed by Scherbaum et al. (2004), while the closest distance to the rupture plane, R_{rup} in CB08, has been estimated with the empirical relationship of Kaklamanos et al. (2011). The depth to the top of the co-seismic rupture plane, Z_{TOR}, and the depth to the 2.5 km/s shear-wave velocity horizon, typically referred to as basin or sediment depth, $Z_{2.5}$, used in CB08, have been estimated with Kaklamanos et al. (2011). The comparison has been made using a vertical strike slip fault, in order to neglect the hanging wall effect present in CB08.

Figure 14 displays the total sigma, as well as its different components, for the considered GMPEs. In general the total sigma's associated to the NGA models are the smallest, the current European model (AB10) and the Greek model (DT07) have intermediate values, while the GMPE developed for Italy (ITA10), Turkey (AC10) and, as consequence, this study have very similar trends and the largest values.

CF08, developed on a global data set, shows large sigma's at short periods and decreasing sigma's at long periods, comparable to the model developed for Europe. The main difference among the models is due to the between-events sigma, which is higher for two regional

Table 5 Main features of the global and regional GMPEs used for the comparisons with the GMPEs derived in this study

GMPE code	M range	Distance range [km]	Style of faulting	Site	Period range [s]
AB10 ~~Pan-EU~~	5–7.6	R_{jb} 0–99	N, R, S~~S~~	Vs_{30} < 360, 360 < Vs_{30} < 760, Vs_{30} > 760	0.05–3.0
BA08 NGA	4.2–7.9	R_{jb} 0–200	N, R, S~~S~~, U	Function of Vs_{30} including non linear effects	0.01–10.0
CF08 global	5–7.2	R_{hypo} 6–150	N, R, S~~S~~	Both EC8 A, B, C, D andFunction of Vs_{30}	0.05–20.0
CB08 NGA	4.0 to 7.5–8.5 (depending on S~~O~~F)	R_{rup} 0– 200	Function including hanging wall effects	Function of Vs_{30} including non linear effects and basin response term	0.01–10.0
DT07 Greece	4.5–6.9	R_{epi} 0–136	N, R, S~~S~~	Rock stiff soft	0.1–4.0
ITA10 Italy	4–6.9	R_{jb} 0–200	N, R, S~~S~~, U	EC8 A, B, C, D, E	0.04–2.0
AC10 Turkey	5–7.6	R_{jb} 0–200	N, R, S~~S~~,	Function of Vs_{30} including non linear effects	0.03–2.0
This study ~~Pan-EU~~	4–7.6	R_{jb} 0–300	N, R, S~~S~~, U	EC8 A, B, C, D	0.02–3.0

GMPEs (ITA10, AC10), the GMPE developed in this study and the CF08 for period shorter than 0.2s.

Finally, the within-event sigmas obtained from the NGA data set are the lowest (CB08 and BA08), while other GMPEs, based on regional or pan-European data sets (ITA10, AC10, DT07, this study) have higher and comparable values.

In Figs. 15 and 16, the comparisons among GMPEs are carried out for sites with Vs30 = 800 m/s and for strike slip style of faulting. Figure 15a shows the median predictions of the global GMPEs in function of magnitude, for PGA and for PSA at T = 2.0 s. The major discrepancies among models are found for PGA, in particular at distances of 100 km, where the NGA models and AB10 predict higher median values than the present study or CF08. At T = 2.0 s, the effect of the magnitude saturation model adopted for this study is evident above the magnitude threshold of 6.5.

Figure 15b shows the median predictions of the global GMPEs in function of distance, for PGA and for ~~SA~~ at T = 2.0 s. The major discrepancies among models are observed for PGA, regardless the magnitude. In particular, it is observed that this study and CF08 have similar PGA attenuation with distance, while NGA models and AB10 predict lower attenuation with distance. At long periods the major discrepancies are found in the near source and for low magnitudes.

Figure 16a shows the median predictions of the regional GMPEs in function of magnitude, for PGA and pseudo spectral acceleration at T = 2.0 s. Major differences are evident at long periods and for small magnitudes and at large distances for both PGA and T = 2.0 s. In particular, the GMPE with the largest difference is the one devel-

Fig. 14 *Top panel*: total standard deviation; *middle panel*: between-events τ standard deviation; *lower panel*: within event ϕ standard deviation of the considered GMPEs. *Continuous lines* are for global or pan-European models; *dashed lines* for regional models, as indicated in the legend of the *top panel*. See Tables 6 and 7 for the explanation of acronyms

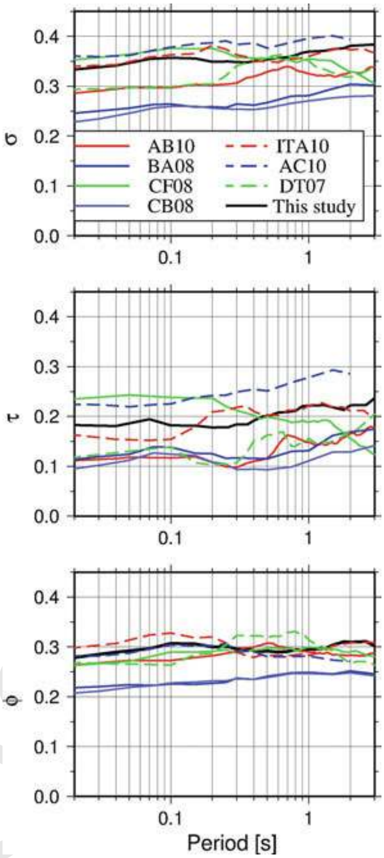

oped for Greece (DT07). Figure 16b shows the median predictions of the regional GMPEs as function of distance, for PGA and PSA at T = 2.0 s. The major discrepancies among models are observed for PGA for small magnitudes and long periods. In particular, at T = 2.0 s the median predictions for Turkey and Italy are lower than the prediction of this study. The GMPE developed for Greece (DT07) shows systematically higher median predictions at distances larger than 10 km, especially at small magnitudes.

7 Discussion

After this study, the following issues can be evidenced:

7.1 Range of applicability of the GMPEs

The GMPEs are strictly usable in their range of applicability (magnitude Mw in the range 4–7.4; distances R_{JB} smaller than 300 km; periods in the range 0.02–3 s).

To this end Fig. 17 (left panel) shows the total standard deviation along with its between- and within-components, ~~are~~ computed for PSA up to 10 s, as included in RESORCE data set. The sharp drop in the different components casts some doubts on the reliability of the

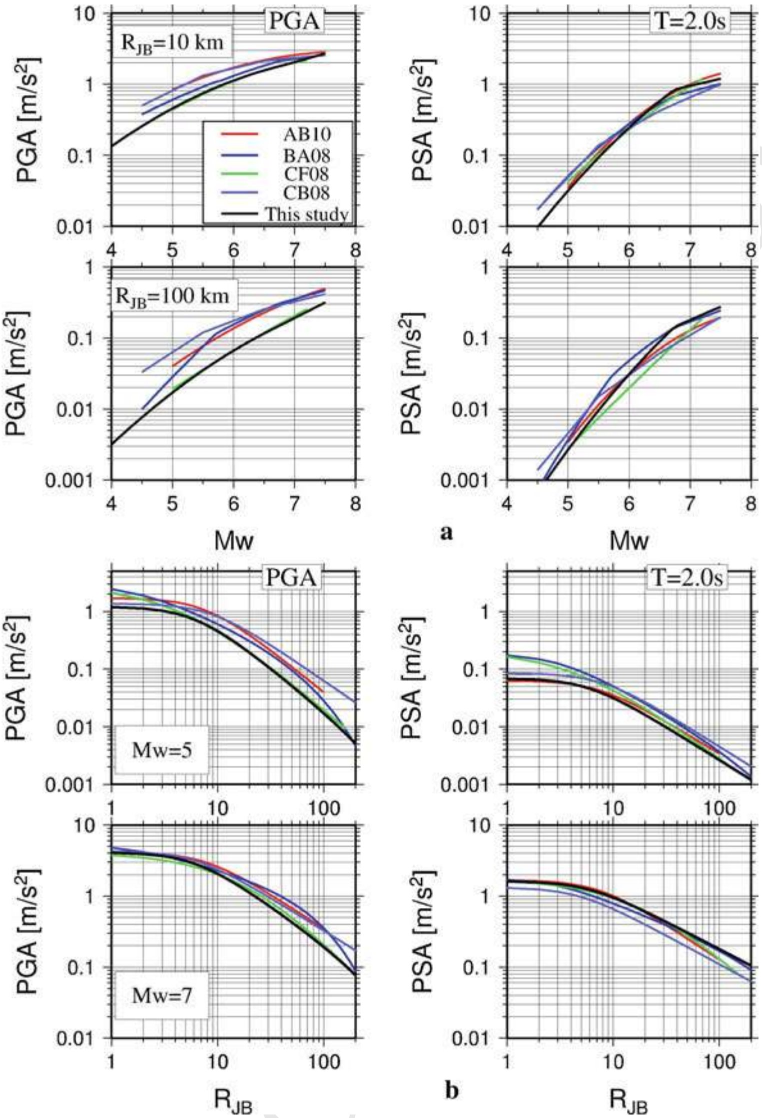

Fig. 15 Global GMPEs: **a** Pseudo spectral acceleration ordinates PSA in function of magnitude; *upper panel PGA* (*left*) and T = 0.2 s (*right*) at a distance of 10 km; *lower panel PGA* (*left*) and T = 0.2 s (*right*) at a distance of 100 km; **b** pseudo spectral acceleration ordinates in function of distance; *upper panel PGA* (*left*) and T = 0.2 s (*right*) for an event of Mw = 5.0; *lower panel PGA* (*left*) and T = 0.2 s (*right*) for an event of Mw = 7. The predictions are computed for Vs30 = 800 m/s^2. See Tables 6 and 7 for the explanation of acronyms

variability captured by the model at periods longer than 3 s. This is confirmed by the increase of the regression coefficient instability at periods longer than 1 s (Figs. 4, 6).

These results could be related both to the reduction in the number of the considered recordings at long period (see Fig. 2, right) and to the processing scheme which was not optimized for long periods.

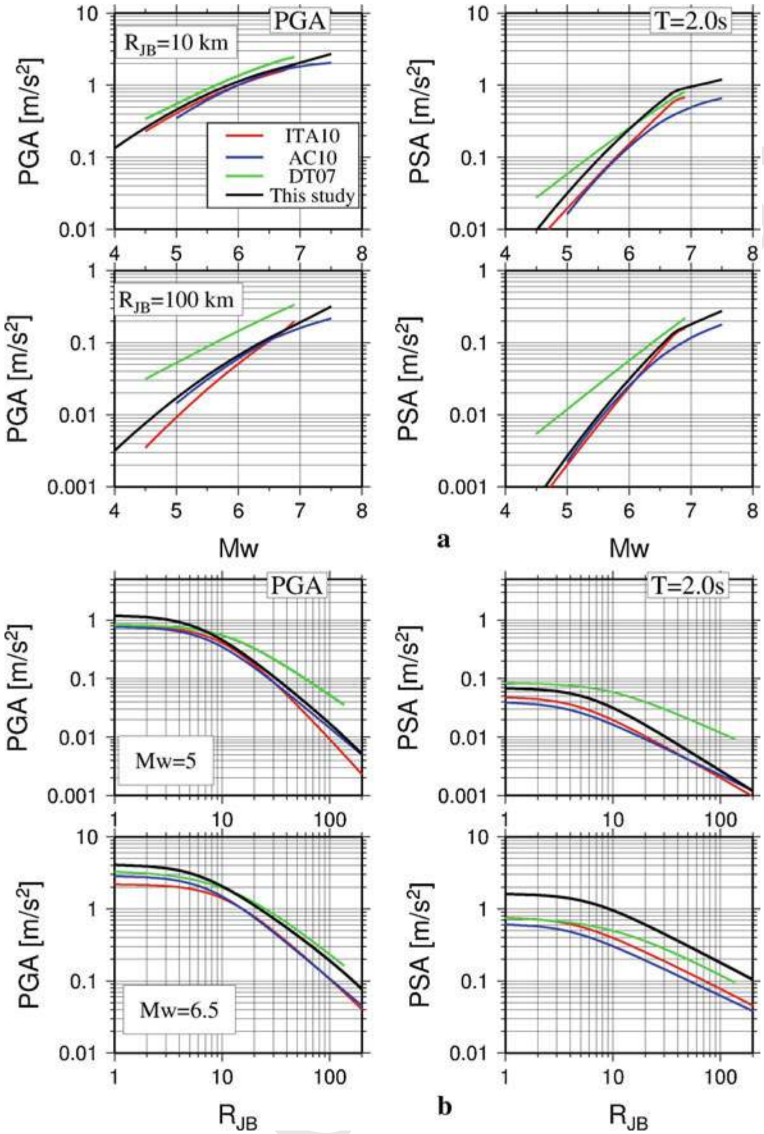

Fig. 16 Regional GMPEs: **a** Pseudo spectral acceleration ordinates in function of magnitude; *upper panel PGA* (*left*) and $T = 0.2\,s$ (*right*) at a distance of 10 km; *lower panel PGA* (*left*) and $T = 0.2\,s$ (*right*) at a distance of 100 km; **b** Pseudo spectral acceleration spectral ordinates in function of distance; *upper panel PGA* (*left*) and $T = 0.2\,s$ (*right*) for an event of $\mathrm{Mw} = 5.0$. *Lower panel PGA* (*left*) and $T = 0.2\,s$ (*right*) for an event of $\mathrm{Mw} = 7$. See Tables 6 and 7 for the explanation of acronyms

7.2 Mainshock /aftershocks

The distributions of the residuals for aftershocks and mainshocks are almost unbiased and with similar sigma (Fig. 10), therefore the features of mainshocks and aftershocks cannot be captured by the empirical ground-motion equations developed for Europe. This can be attributed to the tectonic complexity in Europe, where events belonging to the same

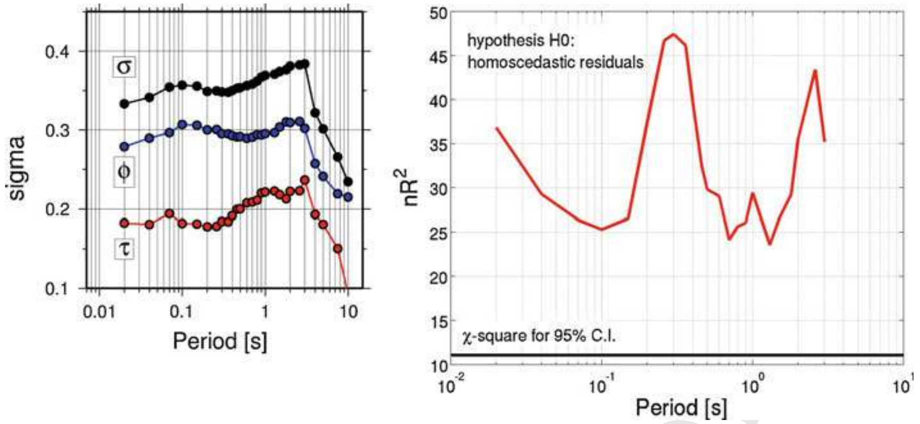

Fig. 17 *Left*: Standard deviations (*black*) along with the between-events (*blue*) and within-event (*red*) components computed up to 10 s. *Right*: Result of the White test applied for testing the null hypothesis of homoscedastic residuals. *Red curve*: nR^2 coefficient of the regression performed over the squared residuals versus the explanatory variable (magnitude and distance), their squares and cross product. *Black line*: the 95 % confidence value for a χ^2 distribution with 6 degree of freedoms indicated that the null hypothesis can be rejected at this level of confidence

seismic sequence frequently occur on adjacent faults (e.g. ~~Umbria-Marche 1997; L'Aquila 2009~~).

7.3 Site characterization and nonlinear site effects

Soil category A (rock) dominates the site-to-site variability for short-periods while for long periods the difference among the classes is less pronounced, with soil sites (classes C and D) showing larger site-to-site variability (Fig. 11). The long period amplifications ($T > 1$s) for classes C or D can be related to both one-dimensional (1D) resonant effects or 2D–3D basin effects (e.g. Rovelli et al. 2001; Bindi et al. 2009b, 2011c), which cannot be captured by any simple site model, based either on the Vs30 or on classes identified by Vs30 intervals (e.g. Luzi et al. 2011).

Non-linear effects are expect to be important for strong shaking at soil sites, that is for large and close earthquakes recorded at sites with low Vs30 values (e.g. classes C and D of EC8). These conditions are not adequately sampled in RESORCE (Figs. 1, 2). The characteristics of the dataset, in terms of magnitude, distance and site ~~characteristics~~, do not evidence non-linear site effects, as shown by the residual distribution in Fig. 13. Therefore a non-linear site model cannot be calibrated with the data set used to derive the GMPEs (see also Akkar and Bommer 2007a,b). Nonlinear models can be only calibrated on external data sets, introducing potential bias in the predictions.

In conclusion, given the RESORCE data set, we preferred to derive a ground-motion model which includes a linear site term. For application where non-linear effects are expected, the predictions of these GMPEs should be corrected by factors calibrated on the specific characteristics of the investigated sites.

7.4 SIGMA

The sigma values obtained in this study are of the same order of the sigma's obtained by the regional models for Turkey and Italy, that mostly contribute to RESORCE (Bindi et al.

2011a; Akkar and Cagnan 2010). These values are larger than sigma's obtained for global or Pan-European GMPEs, which are generally derived for magnitudes larger than 5 (i.e. BA08, CF08, AB10).

The between-events sigma (Fig. 14) of this study is within the values obtained by Akkar and Cagnan (2010, Turkish dataset), and those obtained by Bindi et al. (2011a, Italian dataset) and is generally large for small magnitude events and long periods (Fig. 11). This effect can be ascribed to the large variability of the ground-motion at low magnitudes and/or to the low-cut corner filters applied to the small magnitude events, which have probably introduced low-frequency noise in the analysis. The between-events sigma could also be affected by the conversion into Mw from other magnitude scales.

Figure 17 (right panel) shows the result of a White test (1980) applied to the residual distribution, to test the null hypothesis of homoscedastic residuals. This test is based on the regression of the squared residuals versus the explanatory variables (magnitude and distance in our test), their square and their cross-product. The comparison of the nR^2 coefficient of the regression (red curve in Fig. 17, right) with the critical value for a chi-squared distribution (black line) allows us to reject the null hypothesis of homoscedastic residuals for all periods at 95 % confidence interval. The result of this preliminary test confirms that it is worth to investigate in future the possibility of integrating RESORCE with selected strong earthquakes to constrain a heteroscedastic models over the magnitude range from 4 to 8.

8 Conclusions

We derived a set of GMPEs from ~~a Pan-European data set,~~ RESORCE, compiled in the framework of the project SIGMA (http://projet-sigma.com/organisation.html), ~~to improve the seismic hazard assessment in France~~.

This data set includes the most recent (up to 2011) strong motion data for Europe and Middle East. From the dataset, we extracted a ~~data~~set, named DS-EC8, containing recordings from magnitude and distance ranges wide enough to satisfy a large spectrum of applications: moment magnitudes larger than or equal to 4, hypocentral depths lower than 35 km and Joyner-Boore (R_{JB}) or epicentral (R_{epi}) distances lower than 300 km. The sites are categorized according to the EC8 ground categories (from class A to D), while the style-of-faulting is accounted for as four categories (normal, reverse, strike-slip ~~or~~ unspecified).

A subset of DS-EC8, named DS-VS30, containing only waveforms characterized by known style of faulting and recorded by stations having a measured shear wave velocity profiles, has been used to test of the accuracy of the mean prediction and the variability associated to DS-EC8.

A parametric model has been adopted for the regression of both datasets, following Boore and Atkinson (2008), Bindi et al. (2011a) and Akkar and Cagnan (2010). The predictions associated to the two datasets have similar variability, although the sigma relative to DS-VS30 is slightly smaller than the one relative to DS-EC8 (Fig. 4b). The differences are mainly ascribed to a reduction of the between-events standard deviation, due to the specification of focal mechanisms, and of the site-to-site sigma, due to the knowledge of the subsoil profile, especially at short periods. Both models are reliable, although the one derived from the DS-EC8 dataset has a wider range of applicability, as style of faulting can be unspecified and sites classification can be inferred from surface geology. The median predictions of this study are in agreement with the results of models derived from global data sets at long periods. At short periods (PGA), the model derived in this study shows a better agreement with the Cauzzi and Faccioli (2008) one, while it shows a different rate of attenuation with distance with respect to the considered NGA models. The sigma obtained in this study is larger than sigma's obtained for global or Pan-European GMPEs, which are generally derived for magnitudes larger than 5 (i.e. BA08, CF08, AB10). There is a good agreement with the equations derived for Italy and Turkey, in terms of median and standard deviation at short periods, although the GMPEs derived in this study predict larger ground shaking at long periods.

Considering the sigma values of the model derived in this study, we suggest a revision of the metadata relevant to earthquakes with magnitude < 5, and particular attention should be paid to the conversion from local to moment magnitude for small events, since the between-events sigma for these earthquakes largely contributes to the total variability at long periods. A revision of the high-pass corner frequencies for these earthquakes is also suggested. The evaluation of GMPEs at periods longer than 3 s requires an increase of the number of large-magnitude events, that can be achieved including also earthquakes occurred outside Europe. Moreover, in order to better capture the ground motion variability at different magnitudes, the implementation of heteroscedastic models might be explored.

Finally, the reduction of the epistemic uncertainty affecting the sites might be reached by considering more sophisticated site amplification functions, including for example nonlinear models and basin depth, although there is still a strong limitation of geotechnical information regarding the recording sites, as few data providers in Europe promoted site characterization programs.

Acknowledgments The coefficients of the GMPEs derived in this study and their 95 % confidence intervals are available in the Electronic Supplements of this article, along with some Matlab scripts to compute predictions for different selections of the explanatory variable. Comments from an anonymous Reviewer and from C. Cauzzi triggered significant improvements in the article. The Editor J. Douglas is also acknowledged. The research activities of D. Bindi have been founded through the REAKT (Strategies and Tools for Real Time Earthquake Risk Reduction) EU-FP7 project.

9 Appendix

See Tables 6, 7, 8 and 9.

Table 6 95 % Confidence intervals for the model derived in this study (see Eqs. 1–3) for R_{JB} and EC8 ground categories

T[s~~ec~~]	0.02	0.04	0.07	0.1	0.15	0.2	0.26	0.3	0.36	0.4	0.46	0.5
e1	0.12391	0.121527	0.115083	0.163395	0.157876	0.145339	0.126843	0.145158	0.131924	0.108779	0.148158	0.106598
c1	0.073593	0.084836	0.076821	0.087507	0.086066	0.087099	0.075175	0.056234	0.076841	0.045285	0.080007	0.056646
c2	0.025963	0.022801	0.029608	0.025116	0.031075	0.02521	0.023317	0.024694	0.026571	0.023454	0.030767	0.023685
h	0.705677	0.826334	0.617483	0.754097	0.922982	0.914605	0.7553	0.561224	0.685506	0.637961	0.913656	0.480418
c3	0.000379	0.000421	0.000501	0.000505	0.000528	0.000508	0.000504	0.00043	0.000499	0.000248	0.000383	0.000381
b1	0.061038	0.072102	0.056655	0.067203	0.06722	0.058176	0.06342	0.069368	0.07324	0.061945	0.07168	0.050007
b2	0.013753	0.018276	0.013364	0.013868	0.014396	0.016944	0.016195	0.014831	0.015996	0.014721	0.0169	0.011982
b3	0.015539	0.026582	0.032912	0.038649	0.068145	0.091046	0.089351	0.064411	0.076461	0.075277	0.075031	0.083733
Class A	0	0	0	0	0	0	0	0	0	0	0	0
Class B	0.019884	0.019101	0.023396	0.021834	0.02041	0.018293	0.021751	0.018888	0.014545	0.017174	0.016245	0.018516
CalssC	0.021135	0.019827	0.025217	0.023074	0.024861	0.020882	0.025004	0.022629	0.024476	0.020305	0.019206	0.019526
Class D	0.033404	0.032331	0.043163	0.037048	0.035284	0.041073	0.046337	0.037456	0.029156	0.038351	0.033783	0.033809
sofN	0.050451	0.044131	0.034368	0.046779	0.057222	0.053451	0.06246	0.06278	0.050022	0.050633	0.040136	0.052285
sofR	0.053122	0.048082	0.038819	0.059826	0.065816	0.057652	0.072096	0.064313	0.059711	0.058684	0.049947	0.058154
sofS	0.05393	0.043475	0.032421	0.049164	0.065702	0.051469	0.063086	0.063357	0.054041	0.05164	0.043349	0.050162
sofU	0	0	0	0	0	0	0	0	0	0	0	0

Table 6 continued

T[s~~ec~~]	0.6	0.7	0.9	1	1.3	1.5	1.8	2	2.6	3	~~PGA~~	~~PGV~~
e1	0.135883	0.111665	0.125455	0.125496	0.155883	0.156283	0.102505	0.155931	0.15116	0.182144	0.122927	0.130382
c1	0.046427	0.05541	0.060255	0.045397	0.072641	0.071594	0.056977	0.076385	0.07979	0.109924	0.088425	0.075018
c2	0.029473	0.024827	0.030003	0.027033	0.028322	0.028474	0.026231	0.029861	0.026756	0.031878	0.043311	0.024405
h	0.614371	0.613053	0.723977	0.633978	0.718858	0.875666	0.82935	1.03247	0.896828	1.36986	1.15451	0.604569
c3	0.000311	0.000139	0.000153	9.03E−05	5.26E−05	3.97E−05	7.66E−06	8.94E−05	0.000132	9.26E−05	8.97E−05	0.00047
b1	0.072167	0.044728	0.067567	0.059175	0.073389	0.077649	0.063371	0.076473	0.086585	0.07048	0.100127	0.059753
b2	0.014247	0.01267	0.014035	0.011545	0.016435	0.017151	0.01591	0.017941	0.021173	0.013728	0.021513	0.014809
b3	0.08016	0.08867	0.077122	0.061423	0.070072	0.05788	0.043681	0.002306	0	0	0	0.030284
Class A	0	0	0	0	0	0	0	0	0	0	0	0
Class B	0.023451	0.01943	0.014079	0.019225	0.017356	0.019117	0.011715	0.021086	0.01732	0.026648	0.027186	0.018097
Class C	0.026519	0.021883	0.025502	0.023149	0.018456	0.023132	0.018751	0.019497	0.024489	0.026961	0.026467	0.016873
Class D	0.037533	0.033704	0.042822	0.039871	0.034117	0.052518	0.042387	0.050683	0.05548	0.053011	0.058549	0.043388
SofN	0.044883	0.050114	0.048332	0.064846	0.046582	0.050787	0.059159	0.073939	0.076347	0.061466	0.057963	0.04305
SofR	0.048823	0.057269	0.046387	0.06263	0.057384	0.058538	0.062408	0.077215	0.072066	0.065347	0.059997	0.04705
SofS	0.049879	0.056254	0.049868	0.069784	0.050601	0.055853	0.06573	0.078287	0.07267	0.058471	0.058345	0.04176
SofU	0	0	0	0	0	0	0	0	0	0	0	0

Acceleration is in (cm/s^2), velocity in (cm/s). Values equal to zero correspond to coefficients constrained in the regression

Table 7 95 % Confidence intervals for the model derived in this study (see Eqs. 1–3) for R_{JB} and Vs30 classification

T[s~~ec~~]	0.02	0.04	0.07	0.1	0.15	0.2	0.26	0.3	0.36	0.4	0.46	0.5
e1	0.119376	0.165741	0.114871	0.138983	0.114853	0.15357	0.130826	0.133852	0.119588	0.164146	0.140609	0.147126
c1	0.071763	0.089741	0.067479	0.072709	0.057429	0.089002	0.0773	0.0879	0.067489	0.092358	0.078861	0.070891
c2	0.031129	0.034681	0.030171	0.034202	0.035005	0.034895	0.028872	0.026112	0.024534	0.030809	0.033135	0.038603
h	0.763209	0.75251	0.737684	0.740023	0.682503	1.01786	0.823344	0.804603	0.672935	0.794876	0.723385	0.717549
c3	0.000494	0.00059	0.000405	0.00051	0.000388	0.000521	0.000514	0.000655	0.000404	0.000571	0.000574	0.000452
b1	0.072438	0.085452	0.083027	0.082115	0.079822	0.089221	0.061706	0.069364	0.077476	0.084642	0.090658	0.09876
b2	0.01431	0.018165	0.018655	0.019665	0.016307	0.020788	0.019248	0.01606	0.019264	0.0185	0.018696	0.022122
b3	0.039825	0.037486	0.04596	0.070542	0.099805	0.088819	0.104139	0.072424	0.072665	0.110506	0.096252	0.111751
γ	0.052584	0.045789	0.03917	0.050205	0.03688	0.054365	0.060873	0.045314	0.063349	0.051652	0.058377	0.046624
sofN	0.01437	0.013604	0.013656	0.015221	0.014105	0.010393	0.013403	0.014455	0.01333	0.014434	0.013395	0.013092
sofR	0.021365	0.015231	0.020062	0.017379	0.02124	0.018135	0.021546	0.022927	0.016435	0.023006	0.022461	0.019377
sofS	0.01647	0.01487	0.012361	0.016317	0.016003	0.016366	0.016502	0.017352	0.011701	0.018001	0.014508	0.015469

Table 7 continued

T[s~~ec~~]	0.6	0.7	0.9	1	1.3	1.5	1.8	2	2.6	3	~~PGA~~	~~PGV~~
e1	0.136069	0.161653	0.143452	0.148138	0.13107	0.120361	0.176144	0.196548	0.178821	0.181898	0.175894	0.145007
c1	0.065181	0.083973	0.07617	0.067917	0.069687	0.071903	0.085837	0.096141	0.098345	0.097969	0.091141	0.080703
c2	0.032502	0.035902	0.031267	0.035507	0.027695	0.032235	0.040639	0.048326	0.041525	0.04314	0.048851	0.03229
h	0.722435	0.809068	0.863448	0.942758	0.493574	0.737819	1.09324	1.18635	1.21633	1.97771	1.5161	0.604155
c3	0.000381	0.000298	0.000302	0.000181	9.07E−05	0.000163	0.000124	8.91E−05	0.000256	0.000214	0.000319	0.000508
b1	0.090228	0.088144	0.08326	0.087647	0.081742	0.091426	0.112675	0.111454	0.10073	0.106514	0.133328	0.08088
b2	0.020646	0.018802	0.023769	0.017214	0.021989	0.026164	0.026381	0.02855	0.027099	0.022866	0.035092	0.019505
b3	0.090883	0.09918	0.081987	0.078417	0.070708	0.101311	0.110192	0.067413	0.04185	0.035124	0.03977	0.039424
γ	0.043885	0.061556	0.050754	0.061085	0.047408	0.069918	0.057408	0.059191	0.062944	0.068649	0.075872	0.045541
SofN	0.013892	0.011203	0.010746	0.017231	0.012809	0.014081	0.018581	0.019061	0.01663	0.015954	0.016157	0.01447
SofR	0.018023	0.017466	0.022276	0.024694	0.02027	0.019541	0.027255	0.024237	0.02499	0.028409	0.023208	0.018719
SofS	0.015531	0.01588	0.021322	0.019235	0.017704	0.013794	0.018027	0.016931	0.020535	0.022017	0.019899	0.01403

Acceleration is in (cm/s^2), velocity in (cm/s)

Table 8 95 % Confidence intervals for the model derived in this study (see Eqs. 1–3) for R_{HYPO} and EC8 ground categories

T[s~~ec~~]	0.02	0.04	0.07	0.1	0.15	0.2	0.26	0.3	0.36	0.4	0.46	0.5
e1	0.162223	0.154254	0.189283	0.171375	0.169115	0.17316	0.199215	0.219545	0.1617	0.162699	0.132846	0.141996
c1	0.101039	0.092358	0.097128	0.095642	0.102693	0.108807	0.093717	0.112268	0.078306	0.091217	0.08547	0.060794
c2	0.033926	0.037746	0.037693	0.042037	0.033336	0.035483	0.040852	0.033752	0.029748	0.033652	0.028229	0.028434
h	0.962928	1.19234	1.1525	1.27163	1.24611	1.37899	1.60572	1.50953	1.00863	1.01162	1.30428	0.973498
c3	0.000116	0.000147	0.000286	0.000394	0.000571	0.00058	0.000573	0.000478	0.000297	0.000242	0.000103	0.00019
b1	0.070048	0.075749	0.088331	0.087252	0.07528	0.065611	0.095364	0.076053	0.086192	0.072464	0.075332	0.067039
b2	0.011773	0.012351	0.016414	0.01577	0.015674	0.017542	0.017092	0.014208	0.017884	0.013348	0.016165	0.015296
b3	0.107028	0.103664	0.117345	0.139338	0.121656	0.143074	0.098256	0.119121	0.118327	0.127049	0.109	0.125675
Class A	0	0	0	0	0	0	0	0	0	0	0	0
Class B	0.021473	0.020169	0.022509	0.020515	0.020449	0.019537	0.016488	0.015888	0.021704	0.019351	0.02195	0.027305
CalssC	0.019609	0.024995	0.023025	0.025756	0.020895	0.02229	0.019367	0.018069	0.018154	0.025808	0.023742	0.020612
Class D	0.036033	0.041074	0.045499	0.042577	0.041605	0.045418	0.033054	0.038452	0.039912	0.045533	0.029208	0.039484
sofN	0.042147	0.039597	0.041724	0.044908	0.047293	0.044762	0.056859	0.056113	0.038272	0.052119	0.039565	0.059416
sofR	0.04405	0.043664	0.04608	0.045385	0.055023	0.047656	0.069293	0.054435	0.044668	0.056132	0.04171	0.065653
sofS	0.041382	0.037388	0.041507	0.045641	0.046228	0.047956	0.058056	0.053163	0.045456	0.054731	0.035614	0.061234
sofU	0	0	0	0	0	0	0	0	0	0	0	0

Table 8 continued

T[se~~c~~]	0.6	0.7	0.9	1	1.3	1.5	1.8	2	2.6	3	~~PGA~~	~~PGV~~
e1	0.176433	0.148246	0.136189	0.151171	0.145034	0.158629	0.146203	0.148056	0.200347	0.220246	0.229088	0.104644
c1	0.087692	0.090535	0.081746	0.078289	0.098783	0.068711	0.095043	0.099082	0.112949	0.111766	0.136501	0.07744
c2	0.036387	0.027564	0.031472	0.030833	0.026075	0.039745	0.032644	0.021522	0.039154	0.038436	0.036221	0.031948
h	1.17002	1.15677	2.0927	1.27159	1.819	0.978392	1.85639	1.82087	1.84098	1.89477	1.83951	0.93246
c3	7.32E−05	0	0	1.55E−06	0	0	0	0	0	2.29E−05	0	0.000121
b1	0.086479	0.056097	0.079706	0.078264	0.073053	0.093396	0.070858	0.062862	0.08394	0.103439	0.096826	0.076066
b2	0.015014	0.013019	0.014594	0.01926	0.016978	0.016364	0.014635	0.017022	0.019467	0.020413	0.020473	0.015053
b3	0.100437	0.090815	0.092353	0.106859	0.084317	0.118405	0.102441	0.064018	0.079199	0.011837	0.002244	0.089606
Class A	0	0	0	0	0	0	0	0	0	0	0	0
Class B	0.018676	0.018839	0.013379	0.019991	0.019596	0.022271	0.016666	0.020877	0.019221	0.021426	0.028038	0.016506
Class C	0.023959	0.024281	0.021598	0.01854	0.024414	0.023715	0.022187	0.025692	0.020558	0.02693	0.024545	0.02008
Class D	0.049813	0.040629	0.038765	0.032032	0.040218	0.044745	0.053531	0.055989	0.040841	0.053971	0.07465	0.041802
SofN	0.063185	0.049799	0.066682	0.048557	0.046751	0.058559	0.053649	0.060967	0.080818	0.074659	0.074224	0.045222
SofR	0.066195	0.050842	0.068955	0.058334	0.054271	0.062446	0.061971	0.061758	0.091634	0.071649	0.07204	0.049115
SofS	0.06809	0.052927	0.064046	0.049255	0.045955	0.058149	0.052172	0.061587	0.085699	0.077932	0.069574	0.044288
SofU	0	0	0	0	0	0	0	0	0	0	0	0

Acceleration is in (cm/s^2), velocity in (cm/s). Values equal to zero correspond to coefficients constrained in the regression

Table 9 95 % Confidence intervals for the model derived in this study (see Eqs. 1–3) for R_{HYPO} and Vs30 classification

T[s~~ec~~]	0.02	0.04	0.07	0.1	0.15	0.2	0.26	0.3	0.36	0.4	0.46	0.5
e1	0.148614	0.221493	0.161911	0.127908	0.155409	0.23013	0.228819	0.224915	0.165211	0.147006	0.199166	0.223988
c1	0.077069	0.104547	0.079365	0.077602	0.084072	0.113165	0.123219	0.116923	0.093036	0.078328	0.094014	0.103695
c2	0.048909	0.059291	0.044418	0.037208	0.04363	0.050617	0.05433	0.050143	0.040449	0.038115	0.051277	0.042569
h	1.06658	1.00828	1.12928	1.00474	1.48942	1.34527	1.1677	1.59307	1.12573	1.36232	1.04717	1.46143
c3	0.000316	0.000141	0.000454	0.000468	0.000485	0.00077	0.000753	0.000546	0.000274	0.000134	0.00031	0.000237
b1	0.107778	0.120828	0.099091	0.085023	0.103087	0.116569	0.133753	0.109063	0.098902	0.094054	0.110216	0.126226
b2	0.01887	0.023244	0.01927	0.01913	0.021987	0.022348	0.024811	0.022083	0.02013	0.017234	0.018042	0.024789
b3	0.148945	0.191562	0.147567	0.117771	0.143702	0.163601	0.161578	0.12711	0.168939	0.127675	0.11769	0.115833
γ	5.56E−02	5.53E−02	5.44E−02	5.54E−02	4.38E−02	6.07E−02	4.94E−02	5.36E−02	7.12E−02	5.16E−02	5.97E−02	5.43E−02
sofN	0.012945	0.015325	0.015092	0.010938	0.01641	0.015702	0.013105	0.014415	0.01489	0.012312	0.015086	0.012935
sofR	0.020097	0.01527	0.020411	0.014855	0.019031	0.022561	0.019818	0.025483	0.024511	0.019294	0.021172	0.020085
sofS	0.015127	0.01885	0.013671	0.01232	0.01542	0.015604	0.01503	0.018095	0.017524	0.016167	0.019834	0.017467

Table 9 continued

T[s~~ec~~]	0.6	0.7	0.9	1	1.3	1.5	1.8	2	2.6	3	~~PGA~~	~~PGV~~
e1	0.163636	0.179788	0.257854	0.18107	0.205358	0.2181	0.202476	0.187422	0.208332	0.259683	0.22777	0.154951
c1	0.115852	0.105718	0.102813	0.094651	0.118656	0.129953	0.11866	0.091345	0.103871	0.152804	0.136084	0.085984
c2	0.04157	0.041201	0.060975	0.038254	0.033847	0.047836	0.04956	0.038437	0.048528	0.060871	0.05732	0.033303
h	1.53667	1.36415	1.51506	1.63559	1.78867	1.9574	2.33189	2.03347	2.24876	2.38718	2.38106	1.06636
c3	2.59E−04	0.000247	1.81E−05	1.02E−06	0	0	0	0	0	6.94E−05	0.000177	0.000347
b1	0.060884	0.097142	0.128807	0.099575	0.061382	0.089216	0.107353	0.114807	0.11234	0.142646	0.166586	0.085348
b2	0.021587	0.018132	0.018901	0.020257	0.014423	0.018383	0.022548	0.031173	0.02943	0.033805	0.038534	0.01764
b3	0.159759	0.107094	0.164912	0.119502	0.110014	0.143337	0.174913	0.129941	0.130879	0.097421	0.096057	0.093406
γ	4.67E−02	4.04E−02	6.95E−02	5.67E−02	5.68E−02	6.54E−02	5.22E−02	6.68E−02	6.17E−02	6.44E−02	4.72E−02	4.55E−02
SofN	0.015261	0.017573	0.016388	0.017726	0.017304	0.020619	0.016116	0.018223	0.021319	0.016337	0.018286	0.014969
SofR	0.020816	0.024844	0.027932	0.020622	0.015056	0.025939	0.024476	0.024936	0.030811	0.028956	0.03236	0.022779
SofS	0.015042	0.015076	0.02162	0.014413	0.016785	0.015322	0.022126	0.021087	0.020439	0.021276	0.025577	0.015203

Acceleration is in (cm/s^2), velocity in (cm/s)

References

Abrahamson NA, Youngs RR (1992) A stable algorithm for regression analyses using the random effects model. Bull Seismol Soc Am 82(1):505–510

Akkar S, Bommer JJ (2007a) Prediction of elastic displacement response spectra in Europe and the Middle East. Earthq Eng Struct Dyn 36:1275–1301. doi:10.1002/eqe.679

Akkar S, Bommer JJ (2007b) Empirical prediction equations for peak ground velocity derived from strong-motion records from Europe and the Middle East. Bull Seismol Soc Am 97(2):511–530. doi:10.1785/0120060141

Akkar S, Bommer JJ (2010) Empirical equations for the prediction of PGA, PGV, and spectral accelerations in Europe, the mediterranean region, and the middle east. Seismol Res Lett 81(2):195–206. doi:10.1785/gssrl.81.2.195

Akkar S, Cagnan Z (2010) A local ground-motion predictive model for Turkey, and its comparison with other regional and global ground-motion models. Bull Seismol Soc Am 100(6):2978–2995. doi:10.1785/0120090367

Akkar S, Sandıkkaya MA, Şenyurt M, Azari AS, Ay BÖ (2013) Reference database for seismic ground-motion in Europe (RESORCE), Bull Earthq Eng. ~~Submitted to this issue~~

Al Atik L, Abrahamson NA, Bommer JJ, Scherbaum F, Cotton F, Kuehn N (2010) The variability of ground-motion prediction models and its components. Seismol Res Lett 81(5):794–801. doi:10.1785/gssrl.81.5.794

Atkinson G, Boore D (2011) Modifications to existing ground-motion prediction equations in light of new data. Bull Seismol Soc Am 101:1121–1135

Bindi D, Luzi L, Pacor F (2009) Interevent and interstation variability computed for the Italian Accelerometric Archive (ITACA). Bull Seismol Soc Am 99(4):2471–2488. doi:10.1785/0120080209

Bindi D, Parolai S, Cara F, Di Giulio G, Ferretti G, Luzi L, Monachesi G, Pacor F, Rovelli A (2009b) Site amplifications observed in the Gubbio Basin, Central Italy: hints for lateral propagation effects. Bull Seism Soc Am 99:741–760. doi:10.1785/0120080238

Bindi D, Pacor F, Luzi L, Puglia R, Massa M, Ameri G, Paolucci R (2011a) Ground-motion prediction equations derived from the Italian strong motion database. Bull Earthq Eng 9(6):1899–1920. doi:10.1007/s10518-011-9313-z

Bindi D, Luzi L, Pacor F, Paolucci R (2011b) Identification of accelerometric stations in ITACA with distinctive features in their seismic response. Bull Earthq Eng 9:1921–1939. doi:10.1007/s10518-011-9271-5

Bindi D, Luzi L, Parolai S, Di Giacomo D, Monachesi G (2011c) Site effects observed in alluvial basins: the case of Norcia (Central Italy). Bull Earthq Eng 9:1941–1959

Bommer JJ, Akkar S (2012) Consistent source-to-site distance metrics in ground-motion prediction equations and seismic source models for PSHA. Earthq Spectra 28(1):1–15

Boore DM, Atkinson GM (2008) Ground-motion prediction equations for the average horizontal component of PGA, PGV, and 5%-damped PSA at spectral periods between 0.01 s and 10.0 s. Earthq Spectra 24:99–138

Campbell KW, Bozorgnia Y (2008) NGA ground-motion model for the geometric mean horizontal component of PGA, PGV, PGD and 5% damped linear elastic response spectra for periods ranging from 0.01 to 10 s. Earthq Spectra 24(1):139–171

Cauzzi C, Faccioli E (2008) Broadband (0.05 to 20 s) prediction of displacement response spectra based on worldwide digital records. J Seismol 12(4):453–475. doi:10.1007/s10950-008-9098-y

ComitéEuropéen de Normalisation (CEN) (2004) Eurocode 8: design of structures for earthquake resistance—Part 1: general rules, seismic actions and rules for buildings. Comité Européen de Normalisation, Brussels

Danciu L, Tselentis G-A (2007) Engineering ground-motion parameters attenuation relationships for Greece. Bull Seismol Soc Am 97(1B):162–183. doi:10.1785/0120040087

Douglas J, Halldórsson B (2010) On the use of aftershocks when deriving ground-motion prediction equations. In: Proceedings of the 9th U.S. national and 10th Canadian conference on earthquake engineering, paper no. 220

Douglas J, Akkar S, Ameri G, Bard P-Y, Bindi D, Bommer JJ, Bora SS, Cotton F, Derras B, Hermkes M, Kuehn NM, Luzi L, Massa M, Pacor F, Riggelsen C, Sandıkkaya MA, Scherbaum F, Stafford PJ, Traversa P (2013) Comparisons among the five ground-motion models 1 developed using RESORCE for the prediction of response spectral accelerations due to earthquakes in Europe and the Middle East, Bulletin of Earthquake Engineering, this issue

Efron B, Tibshirani RJ (1994) An introduction to the bootstrap. Chapman & Hall/CRC, Boca Raton, Florida. ISBN 978-0412042317, 456 pp

Foti S, Parolai S, Bergamo P, Di Giulio G, Maraschini M, Milana G, Picozzi M, Puglia R (2011) Surface wave surveys for seismic site characterization of accelerometric stations in ITACA. Bull Earthq Eng 9:1797–1820

Gardner JK, Knopoff L (1974) Is the sequence of earthquakes in Southern California, with aftershocks removed, Poissonian? Bull Seis Soc Am 64:1363–1367

Ghasemi H, Zare M, Fukushima Y (2008) On the scattering in normal distribution of the peak ground acceleration residuals in Alborz region, 14th World Conference on Earthquake Engineering, October 12–17. Beijing, China

Kaklamanos J, Baise LG, Boore DM (2011) Estimating unknown input parameters when implementing the NGA ground-motion prediction equations in engineering practice. Earthq Spectra 27(4):1219. doi:10.1193/1.3650372

Luzi L, Bindi D, Franceschina G, Pacor F, Castro RR (2005) Geotechnical site characterisation in the Umbria-Marche area and evaluation of earthquake site-response. Pure Appl Geophys 162:2133–2161. doi:10.1007/s00024-005-2707-6

Luzi L, Puglia R, Pacor F, Gallipoli MR, Bindi D, Mucciarelli M (2011) Proposal for a soil classification based on parameters alternative or complementary to Vs, 30. Bull Earthq Eng 9(6):1877–1898. doi:10.1007/s10518-011-9274-2

Menke W (1989) Geophysical data analysis: discrete inverse theory. In: Dmowska R, Holton JR (eds) IntGeophys series, vol 45. Academic Press, New York, p 289

Rovelli A, Scognamiglio L, Marra F, Caserta A (2001) Edgediffracted 1-sec surface waves observed in a small-size intramountainbasin (Colfiorito, central Italy). Bull Seismol Soc Am 91:1851–1866

Scherbaum F, Schmedes J, Cotton F (2004) On the conversion of source-to-site distance measures for extended earthquake source models. Bull Seismol Soc Am 94(3):1053–1069

Tatar M, Jackson J, Hatzfeld D, Bergman E (2007) The 2004 May 28 Baladeh earthquake (Mw 6.2) in the Alborz, Iran: overthrusting the South Caspian Basin margin, partitioning of oblique convergence and the seismic hazard of Tehran. Geophys J Int 170:249–261

White H (1980) A Heteroskedasticity-consistent covariance matrix estimator and a direct test for heteroskedasticity. Econometrica 48(4):817–838

Yenier E, Sandıkkaya MA, Akkar S (2010) Report on the fundamental features of the extended strong-motion databank prepared for the SHARE project. Report WP4—strong ground-motion modeling. Project SHARE http://www.share-eu.org/node/73